Degassing and Deformation of the Pantelleria Magma Chamber

Gareth Fabbro
Fitzwilliam College
Supervisor: Marie Edmonds

8 January 2010

Acknowledgements:

I would like to thank David Neave, for his company on Pantelleria and his stimulating conversation (both geological and otherwise); Mike Hall for running the carbon isotope data; Richard Herd for guiding us around the island; and especially Marie Edmonds for all the hard work she has put in as my supervisor.

This report contains 7 453 words, not including captions, tables, references and appendices.

Abstract

Fieldwork was undertaken to survey CO_2 flux from the flanks of Pantelleria, a quiescent volcano in the Sicily Channel. An area of 0.163 km^2 was chosen around Favàra Grande, as this was an area of active degassing in previous studies and is at the centre of the deflation seen to occur on the island. Flux measurements were taken using an accumulation chamber method, and samples were also brought back to Cambridge to analyse for $\delta^{13}C$. The total anomalous CO_2 flux was found to be 1 300 kg d^{-1}, with an average of 15.6 g m^{-2} d^{-1}. Precision test were carried out, and the results are considered accurate to 8 %, however there was also an increase of ∼70 % over a period of a week, possibly due to meterological conditions. The $\delta^{13}C$ of the CO_2 was found to be –7 ‰, close to the magmatic $\delta^{13}C$.

Pantelleria is currently undergoing a period of deflation, although there was an episode of inflation preceding the 1891 eruption, and others ∼500 and ∼900 years ago. The amount of gas currently escaping the magma chamber was found to be too little to fully explain the deflation, although the CO_2 flux from Favàra Grande may be have been decreasing over the last ten years. Because the magma chamber is large and shallow, small changes in temperature lead to large effects at the surface. A temperature change of 0.001 K yr^{-1} is large enough to explain the deflation through thermal contraction. The deflation is therefore likely caused by a combination of both degassing and the thermal contraction of the magma chamber.

Contents

1. Introduction

1.1 Geological Setting

Pantelleria is a small volcanic island in the Sicily Channel. It last erupted in a small, submarine eruption off the Northwest coast in 1891 (Butler, 1892).

It sits at the northwest end of the Pantelleria Graben, one of several troughs that run roughly northwest–southeast in the Sicily Channel (figure 1.1). These formed by extension during Late Miocene-–Early Pliocene (Civile et al., 2008). The current direction of extension is east–west, and is consistent with paelomagnetic readings showing Sicily to have rotated 15° counterclockwise relative to Africa since the Pliocene (Reuther and Eisbacher, 1985).

Crustal thinning under Pantelleria is shown by both the bouguer anomaly (Berrino, 1997) and seismic profiles (Civile et al., 2008). The crust thins to 17km in the Pantelleria graben, while it is 30-40km thick under Africa and Sicily. This likely explains the presence of a magma chamber under the island.

Most of the volcanism on Pantelleria is strongly peralkaline (Mahood and Hildreth, 1986), with Foerstner (1881) introducing the name pantellerite to describe the most strongly peralkaline. Peralkaline rocks have a lower concentration of Al_2O_3 than Na_2O and K_2O combined, with MacDonald (1974) suggesting the somewhat arbitrary definition of pantellerities as containing concentrations of Al_2O_3 less than $1.33 \times$ Fe (as FeO) + 4.40. Pantellerites also occur in other continental rifts, such as the East African rift (Macdonald and Scaillet, 2006) and the Taupo Volcanic Zone in New Zealand (Houghton et al., 1992). There are also some alkali basalts, mainly in the northwest of the island.

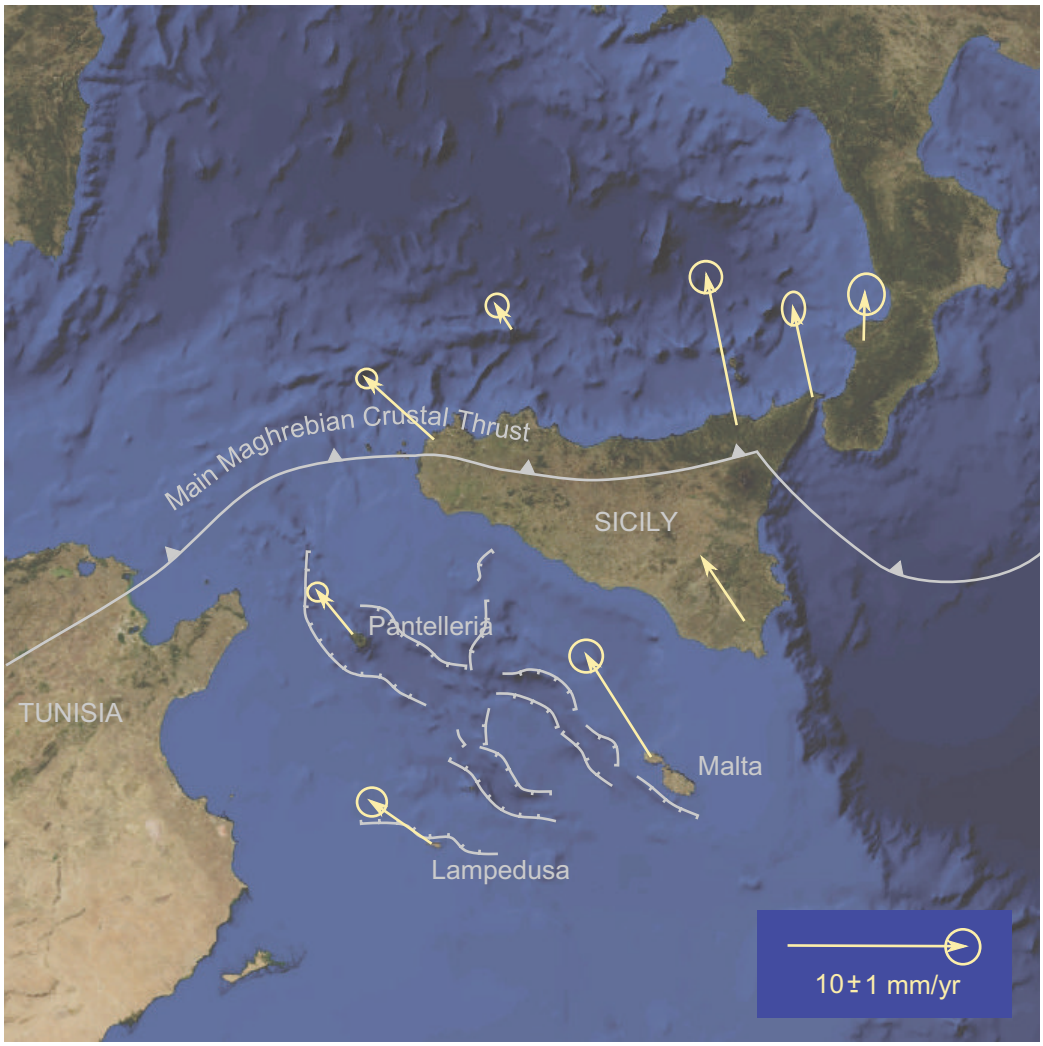

Figure 1.1: Location of the island of Pantelleria, with the main tectonic structures shown. Arrows represent GPS velocities relative to Eurasia. Modified from Catalano et al. (2009) with GPS velocities taken from Hollenstein et al. (2003).

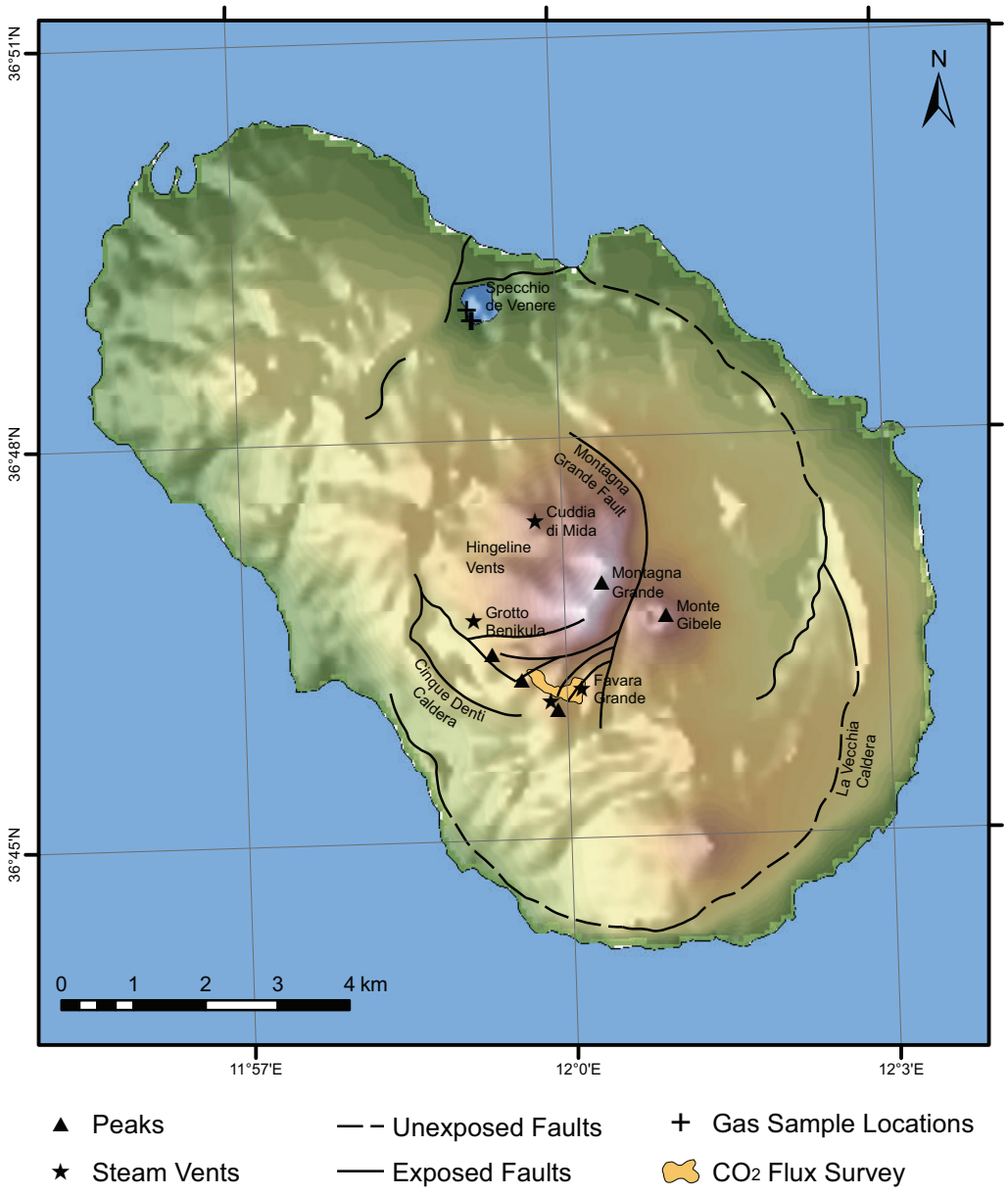

Figure 1.2: Sketch map of the island showing the main volcano-tectonic features. Modified from Mahood and Hildreth (1986), DEM taken from the SRTM (2007). Coordinates are relative to the European Datum 1950, as are the coordinates of all following diagrams.

1.2 Volcano-tectonic Features

The island has at least two calderas (Civetta et al., 1988; Cornette et al., 1983; Mahood and Hildreth, 1983) (figure 1.2). The earlier has been named the La Vecchia caldera and is dated at using K–Ar 114 ka, assuming welded ignimbrite Unit Q was erupted during its formation (Mahood and Hildreth, 1986). Bracketing units place it between 175 ka and 106ka. The younger is located differently by Mahood and Hildreth and Cornette et al. (1983). It is named the Cinque Denti or the Monestero caldera by respective authors, the notation of Mahood and Hildreth is used here. Both calderas can be seen quite clearly on the south of the island (figure 1.3).

The younger caldera collapsed during the eruption of the Green Tuff (45 ka), a distinctive marker bed that covers much of the island. It has been correlated with the Y-6 ash band found in boreholes across the Mediterranean, and has been found as far away as Lesvos Island in Greece (Margari et al., 2007).

After the Green Tuff eruption, Monte Gibele was formed by a series of trachytic eruptions. The pantellerites are related to the trachytes by fractional crystallisation, with pantellerite being more evolved. The flows on Montagna Grande originated from the vent at the top of Monte Gibele. Montagna Grande was then uplifted as a block, in a 'trapdoor' style (figure 1.4) (Mahood and Hildreth, 1983). Villari (1970, 1974) and Wright (1980) suggested Montagna Grande was an endogenous dome, however its stratified nature and the similarity to the trachytes of Monte Gibele and the pattern of faults strongly supports the uplifted block hypothesis.

Resurgence is common in caldera-forming eruptions, and usually forms domes. The resurgence on Pantelleria shares many features with that seen at Ischia in the bay of Naples (Molin et al., 2003; Orsi et al., 1991). The block-like nature of the uplift, rather than the more common doming, is likely due to the large ratio of overburden thickness to the diameter of the caldera (Acocella et al., 2001; Cole et al., 2005). The uplift could either be due to isostatic re-equilibration or a renewed melt input. Mahood and Hildreth suggest that the eruption of Monte Gibele compensated for the mass

(a)

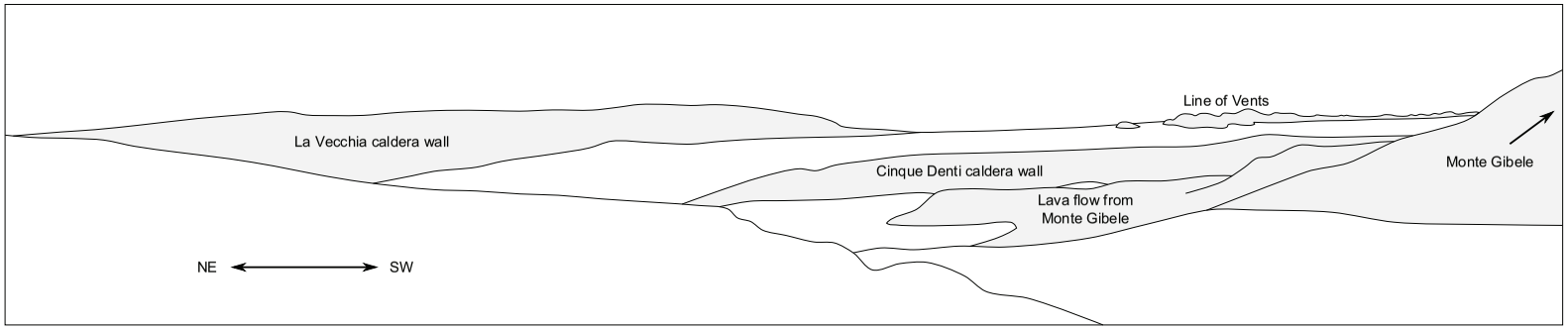

(b)

Figure 1.3: (a) Photo and (b) diagram drawn from the photo showing the two caldera walls visible on the south of the island. Taken from 12° 01' E 36° 47' N, looking south east.

lost during the Green Tuff eruption and therefore the uplift must be due to an injection of melt. Analogue models by Acocella et al. also assume an injection of melt.

The uplifted block is delineated by the Montagna Grande fault in the east and the north, by the line of recent pantelleritic cones of Monte Gibile and Fossa del Russo in the south and by the hingeline volcanics in the west. The displacement was greatest in the east, estimated as 275 m by Mahood and Hildreth, mostly taken up by the Montagna Grande fault. In the west there was little movement, causing the entire block to tilt. There was, however, some faulting in the west, creating a conduit for magma to reach the surface at numerous hingeline vents. The volcanics associated with uplift were erupted between 18 000 and 3 000 years before present (Mahood and Hildreth, 1986).

The geology of the area around Favàra is dominated by the uplift of Montagna Grande. The Montagna Grande Fault runs to the east of the are studied, but splays into several strands (figure 1.5). Some of these strands run through the area studied, and these control the location of many of the volcanic features present. Monte Gibile and Fossa del Russo erupted at points where faults cross, and the steam vents also occur above faults.

There is evidence for a large, active magma chamber beneath Montagna Grande. There are numerous fumaroles and hot springs around the island, and a geothermal anomaly centred on Montagna Grande (Squarci et al., 1994). Geodetic measurements suggest a deflating chamber centred at 4.5 km depth (Mattia et al., 2007). Petrological evidence suggest a silicic magma chamber with the top at 3.6 km (Gioncada and Landi, 2010). This is likely to be the chamber responsible for the Green Tuff eruption and the formation of the Cinque Denti Caldera. The volume of the Cinque Denti caldera has been estimated as 3.4 km^3 (Mahood and Hildreth, 1986), and the volume of the Y-6 ash layer associated with the collapse at 10 km^3 of dense rock equivalent (Margari et al., 2007). As eruptions are rarely thought to empty more than 10 % of the magma chamber, the size of this chamber is likely to be at least 30 km^3. There may also be a deeper, basaltic magma chamber at 7 km depth (Gioncada and Landi, 2010).

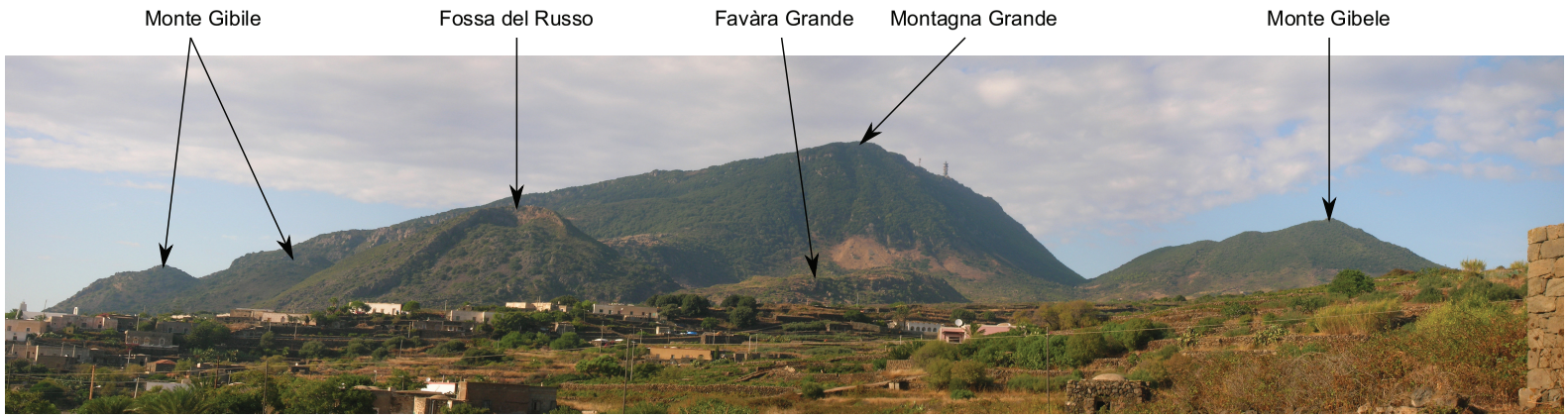

Figure 1.4: View of Motagna Grande and Monte Gibele. The Montagna Grande Fault, which took up most of the uplift, runs between the two. The line of pantelleritic cones that deliminate the south side of the 'trapdoor', Monte Gibile and Fossa del Russo, are also visible. Taken from Cuddia Attalora, 12° 01' E 36° 45' N, looking north.

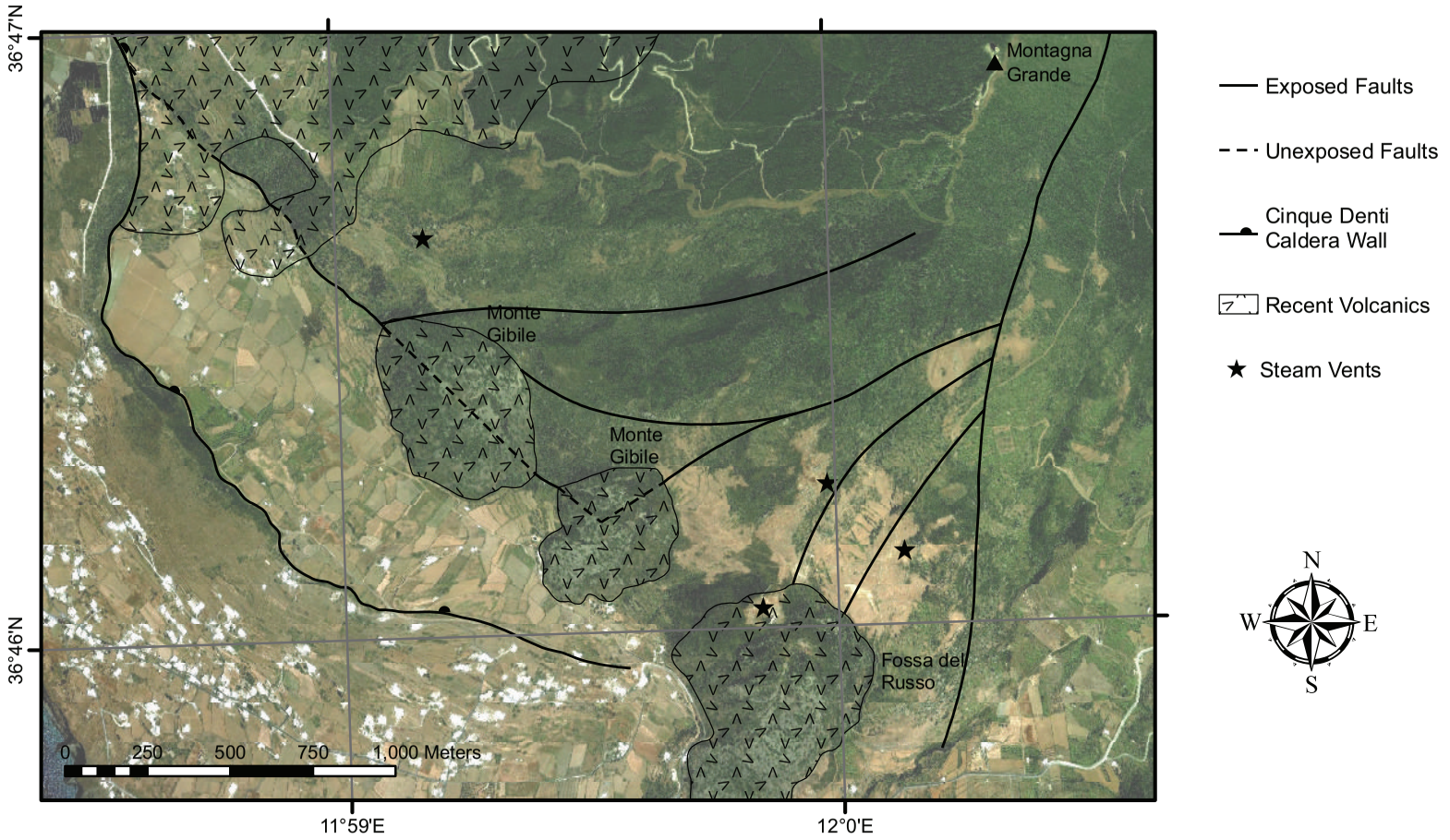

Figure 1.5: Geology of the area around Favàra Grande. Aerial photo from Google Earth, geology modified from Mahood and Hildreth (1986).

1.3 Aims

Although Pantelleria is in a quiescent period there is still the chance of a major eruption. The two calderas are evidence of massive past eruptions with the potential to effect much of southern Europe and north Africa. Ash from the last caldera forming event has been found as far away eastern Greece. CO_2 emissions show that the magma chamber under the island is still active.

CO_2 is a hazard on volcanoes. As it is denser than air, it sinks and can collect in hollows and depressions. This can suffocate people and animals. The aim of this project was to quantify the CO_2 flux and spatial distribution from one area of Pantelleria. While the entire island has been surveyed for CO_2 flux (Favara et al., 2001), the resolution was to low to pick out which geological features were controlling the spatial distribution. The area around Favàra Grande was chosen as it was found to be one of the areas of greatest CO_2 degassing by Favara et al., as well as the site of several fumaroles.

The island is also actively deforming, and currently undergoing a 30 year period of deflation. Better constraints on the CO_2 flux can reveal whether it is a possible mechanism to explain this. Relating the CO_2 flux to particular faults can also provide evidence that they are active in this current phase of deformation.

2. Data Collection

Fieldwork was carried out over 13 days between 29 August and 11 September 2009.

2.1 CO_2 Flux Measurements

The area of Costa della Favàra and Passo del Vento was chosen to preform a detailed survey of the soil CO_2 flux (figure 1.2). This area was fairly flat, having been terraced for farming in the past. It contained three active steam vents — La Favàra Grande, Fossa del Russo and another on a ridge north of Passo del Vento — along with sulphur deposits indicating it was an area of secondary volcanic activity. This site was also close to the surface expression of the depressurising magma source postulated by Bonaccorso and Mattia (2000) and Mattia et al. (2007) from deformation data.

Flux readings were made using the accumulation chamber method (Chiodini et al., 1998). CO_2 flux was measured, along with concentrations and temperatures, with a LI-8100 Automated Soil CO_2 Flux System. This consisted of a non-dispersive infra-red (NDIR) gas analyser attached to a survey chamber, which was placed over a collar inserted into the soil. The analyser was controlled by a palmtop connected by a serial cable.

The majority of readings were taken between the 2–5 September, with precision tests carried out later in the week.

2.1.1 Flux Calculations

As the concentration in the chamber increases, the concentration gradient between the soil and the chamber decreases. The flux is proportional to the concentration gradient, so also decreases as the measurement continues (figure 2.1). It is therefore necessary to calculate the flux at the instant the chamber closed. The flux was calculated assuming an exponential form for

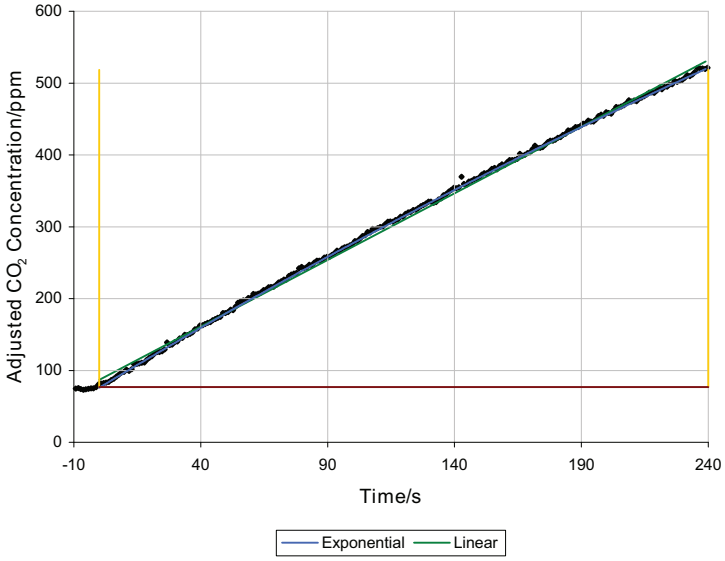

Figure 2.1: Plot of a typical flux measurement. Yellow lines represent the start and stop times, and the brown line the initial CO_2 concentration used in the calculation. CO_2 concentrations adjusted to take into account the water concentration.

the concentration of CO_2 with time, rather than a linear form as it gives a more accurate answer.

Calculations were made using the software shipped with the LI-8100. Only measurements after stable mixing was established — with smooth, steadily increasing concentrations — were used in the calculations. In the field this was assumed to be 10 s after the chamber closed until it opened again, but on return these times could be adjusted after viewing the graphs. The CO_2 concentrations were adjusted to remove the affect of water vapour, and fit to the equation:

$$C(t) = C_x + (C_0 - C_x)\, e^{-at}$$

where $C(t)$ is the CO_2 concentration as a function of time, C_0 is the initial CO_2 concentration, t is the time in seconds and C_x and a are calculated constants that define the asymptote and curvature respectively (LI-COR Inc, 2007). Differentiating this to get the flux, we can find the flux at the

instant the chamber closed:

$$\frac{\mathrm{d}C}{\mathrm{d}t} = a\left(C_x - C_0\right)e^{-at}$$

$$\left.\frac{\mathrm{d}C}{\mathrm{d}t}\right|_{t=0} = a\left(C_x - C_0\right)$$

2.1.2 Length of Measurment

The instruction manual (LI-COR Inc, 2007) claimed that 2 minutes would be enough to measure the flux accurately. However, in initial tests found that CO_2 concentration often didn't start to rise until 5–6 minutes into the reading (figure 2.2a). Later readings do not have this delay (figure 2.2b), and measurement length was reduced to four minutes. This could have been due to a partial blockage in the instrument that cleared itself during th course of the survey. This could explain some of the longer-term variation found (page 22), however the larger differences were located in the area surveyed without the delay.

One downside of the longer measurement times was that CO_2 could build up in the soil under the chamber while it was closed (figure 2.3). This happens because the CO_2 concentration in the chamber is greater than the concentration in the atmosphere, so the rate of diffusion out of the soil is lowered. The regression technique used to calculate the flux calculates the initial flux, therefore this build up of CO_2 should not affect the result during a single measurement. However, some of the repeat measurements taken shortly after an initial reading may be affected, especially where there were large fluxes.

2.1.3 Limitations on Survey Sites

The survey chamber required soil to allow the collar to be inserted, ruling out rocky areas. Steep slopes also had to be avoided as the chamber wouldn't stand upright at too great an angle. Also, the soil level inside the collar had to be close to perpendicular to the collar. This was in order to properly estimate the volume of air inside the system, needed in the calculation of the

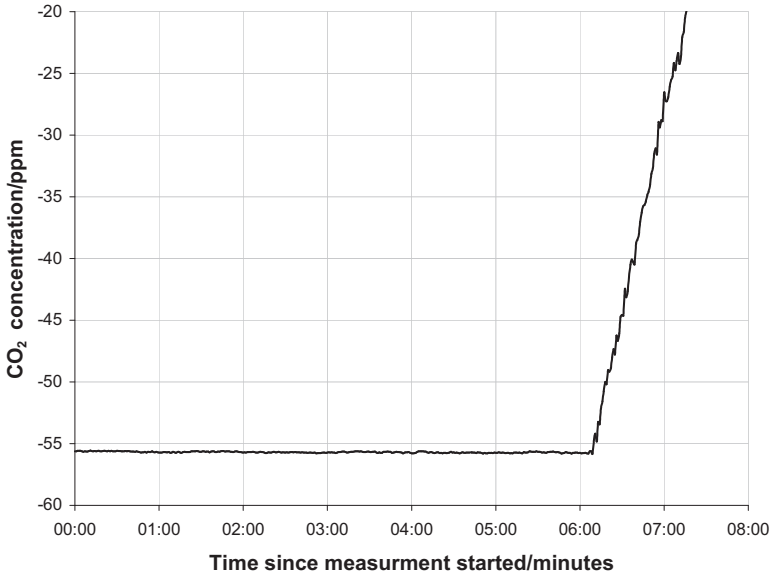

(a) CO_2 concentrations for measurement 035. Flux at site was 13.3 ± 1.1 g m^{-2} d^{-1}.

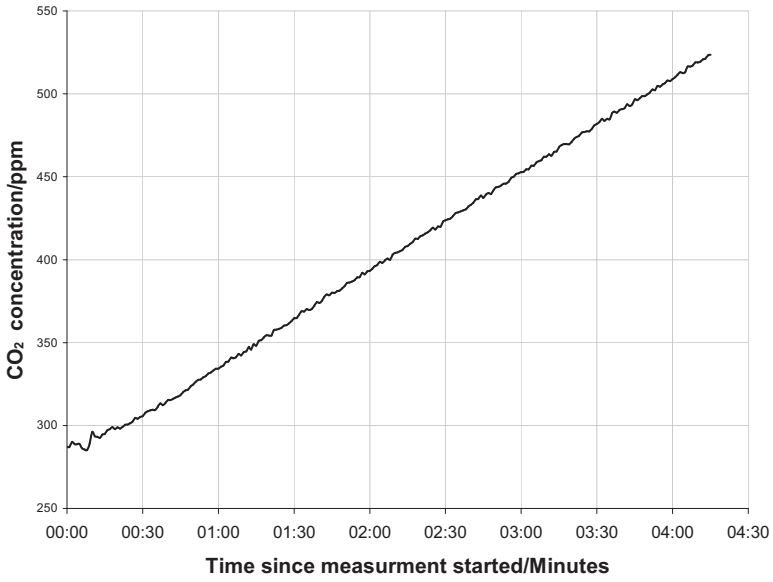

(b) CO_2 concentrations for measurement 276. Flux at site was 25.8 ± 2.1 g m^{-2} d^{-1}.

Figure 2.2: CO_2 concentrations (corrected for for water vapour dilution). Notice the large delay before CO_2 concentration begins to increase in (a).

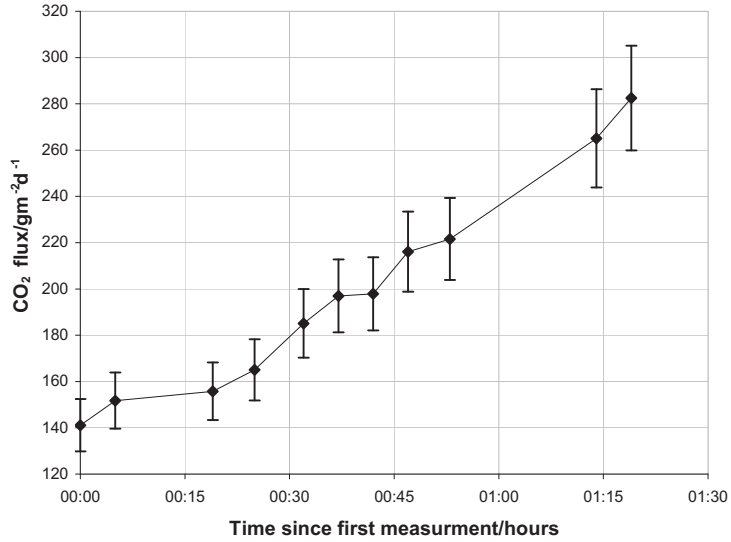

Figure 2.3: Increase of CO_2 flux with repeated readings due to the build-up of CO_2 in the soil beneath the survey chamber. The chamber was closed for measurements for four minutes, with a one minute pause with the chamber open between readings.

flux.

Excessive vegetation was also a problem. In parts of the survey site it was close to impenetrable, making measurements impractical. These factors conspired to rule out some areas of interest. The three cones of Monte Gibile and Fossa del Russo are the most recent extrusive activity in the area, and as such may still be areas of active degassing. Despite this, it was not possible to measure the CO_2 flux from these, as they were steep, rocky and thickly vegetated. Similarly Cùddia di Mida (figure 1.2) was identified by Favara et al. (2001) as an area of high soil CO_2 flux, yet was not a practical site for a survey.

2.1.4 Reproducibility

The stated error for CO_2 flux measurement on the LI-8100 is 1.5% (LI-COR Inc, 2007). However, in the field other sources of error could effect the final reading. Several sites were chosen in order to get aa representative selection

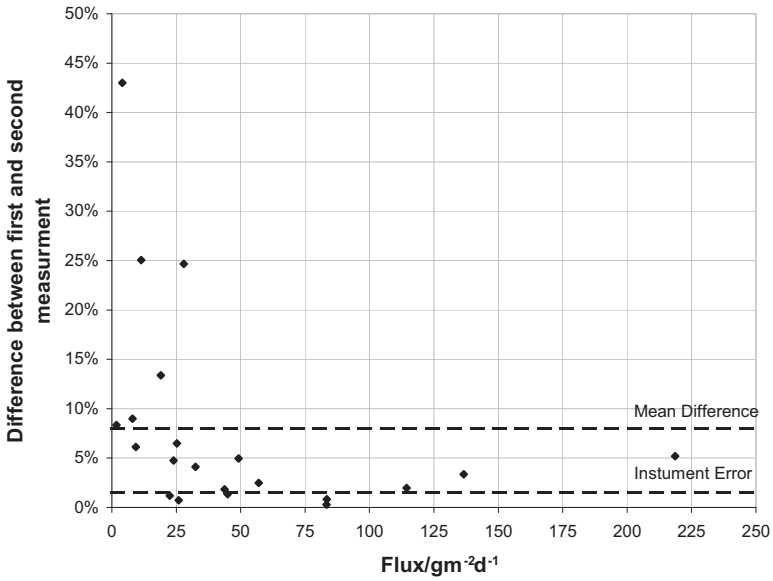

Figure 2.4: Difference between multiple readings taken at the same point, plotted against CO_2 flux.

of conditions and fluxes. At these sites the readings were repeated, after allowing at least a minute for the CO_2 concentrations in the soil to return to normal. The differences between the first and second reading are plotted in figure 2.4.

Apart from at small fluxes (below 30 g m^{-2} d^{-1}), the variation is low and the mean variation of 8% gives a reasonable estimate of the errors. The larger difference in the reproducibility compared to the instrument error could be a real variation in the degassing, over time periods of a few minutes. It could also be due changes in conditions at the near-surface, such as wind strength. The variation is just as likely as to be positive as negative (the sum of the 21 differences is only 1.05 g m^{-2} d^{-1} or 0.38 % of the sum of the fluxes), suggesting that this is not a systematic variation between readings.

In order to check the variations over a slightly longer period, several sites were revisited towards the end of the week, and the flux was measured again (table 2.1). At every site the flux increased, sometimes more than doubling (figure 2.5). Linear regression shows that the average increase in flux was

Table 2.1: CO_2 Fluxes for repeat measurements

Site 1			Site 2			Distance	CO_2 Flux/g m^{-2} d^{-1}			
Coordinates		Date	Coordinates		Date	/m	Site 1	Site 2	Mean	Difference
32381	73573	03/09/09	32390	73582	10/09/09	12.7	23.96	83.43	53.69	59.47
32376	73529	03/09/09	32372	73534	10/09/09	6.4	43.71	134.38	89.04	90.67
32349	73581	03/09/09	32343	73581	10/09/09	6.0	0.00	19.20	9.60	19.20
32273	73450	04/09/09	32275	73449	10/09/09	2.2	0.00	37.76	18.88	37.76
32221	73425	04/09/09	32221	73423	10/09/09	2.0	13.08	47.42	30.25	34.34
67380	73561	05/09/09	67387	73558	10/09/09	7.6	179.17	255.79	217.48	76.62
67381	73600	05/09/09	67386	73598	10/09/09	5.4	97.80	187.16	142.48	89.36
67264	73680	05/09/09	67266	73681	10/09/09	2.2	37.53	68.52	53.02	30.99
67632	73409	06/09/09	67632	73410	10/09/09	1.0	64.17	69.66	66.91	5.49
67455	73498	06/09/09	67455	73503	10/09/09	5.0	16.69	251.21	133.95	234.51

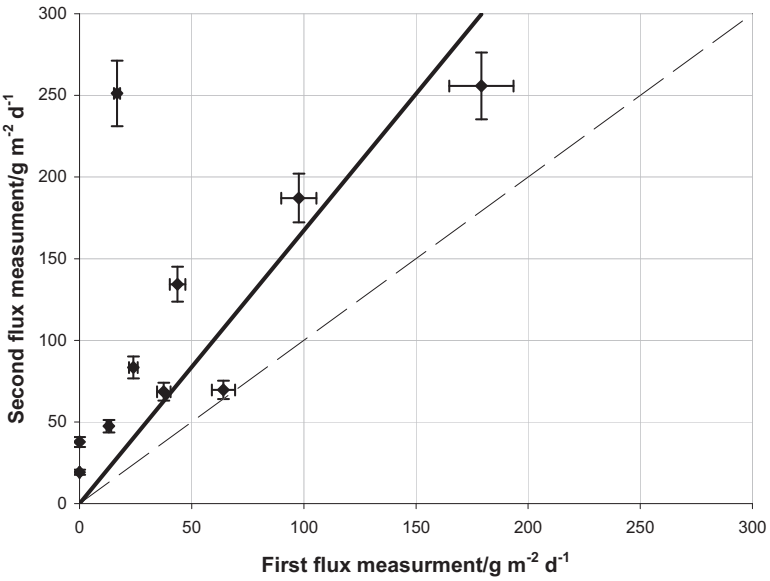

Figure 2.5: Repeat measurements of CO_2 flux at selected sites. Error bars are 8% of reading. Solid line is a linear regression with a gradient of 1.7, dashed line is 1:1.

about 70 %.

This is unlikely to be measurement error. It is far larger than the short term variations, and always increased. This may be due to a change in the rate of magma degassing, however the second series of measurements were taken shortly after a heavy rain storm whereas all other readings were taken after a long, dry spell. CO_2 is soluble in water, so rain would be expected to lower the flux rate. However, some long-term measurements taken on Vesuvius have shown peaks after rain (Granieri et al., 2010). This is possibly due to funnelling of gas by an impermeable layer of groundwater. Also, when the first set of readings were taken on the western half of the area there was a strong wind, but during the second set of readings it was still. Strong winds can infiltrate the upper layers of soil, reducing the CO_2 concentrations and hence fluxes (Healy et al., 1996; Lewicki et al., 2007). Other meteorological effects, such as humidity and air pressure, can also have an affect on the flux of CO_2 at the surface (Badalamenti et al., 2004; Chiodini et al., 1998).

2.1.5 Collar Insertion

Placing the chamber on the surface leads to the distortion of the CO_2 gradient in the soil, which in turn can effect the result (Healy et al., 1996). This can be lessoned by inserting a collar into the soil.

On hard ground, this collar could only be inserted a few millimetres, however it still preformed an important duty by sealing the chamber to the ground. Figure 2.6 shows the effect of not inserting the collar on the concentration of CO_2 in the chamber. With the collar there is a steady accumulation of CO_2, which is not seen when the collar is not in place. There were gaps between the base of the chamber and the ground, allowing the chamber air to mix with the atmosphere. The effect was not as pronounced on loose ground.

Inserting the collar disturbed the ground, and on loose ground this caused an increase in the CO_2 flux that decayed exponentially with time (figure 2.7). On hard ground, inserting the collar had little effect, probably because the collar couldn't be inserted as deep and much less of the soil was disturbed.

In order to allow the flux to settle back to original values, several survey sites were set up at once. This gave between 30 minutes and and hour between collar insertion and flux measurement. However, at 30 minutes the measured flux could still be up to 20 % higher than the true flux. Most readings were taken on hard ground and left for over 30 minuts, so the effect would have been minimal.

2.1.6 Temperature Variations

The temperatures measured by the spectrometer did not reflect the temperature of the gasses escaping, instead measuring the ambient temperature of the atmosphere. This is apparent from figure 2.8(a), which also shows the greatest variation in temperatures during measurements was during the middle of the day. This variation is caused by the sun heating the chamber, as can be see in figure 2.8(b). The only place where the temperature of the gasses influenced the temperature of the chamber was at site 15, on steaming ground in Passo del Vento. This is where the highest flux of 1900 g m^{-2} d^{-1} was recorded, and the chamber temperature reached 45 °C. The temperature

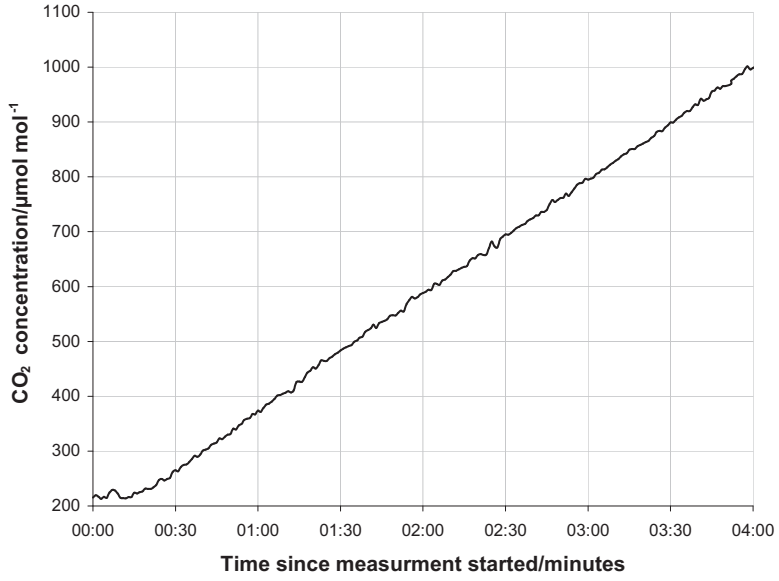

(a)

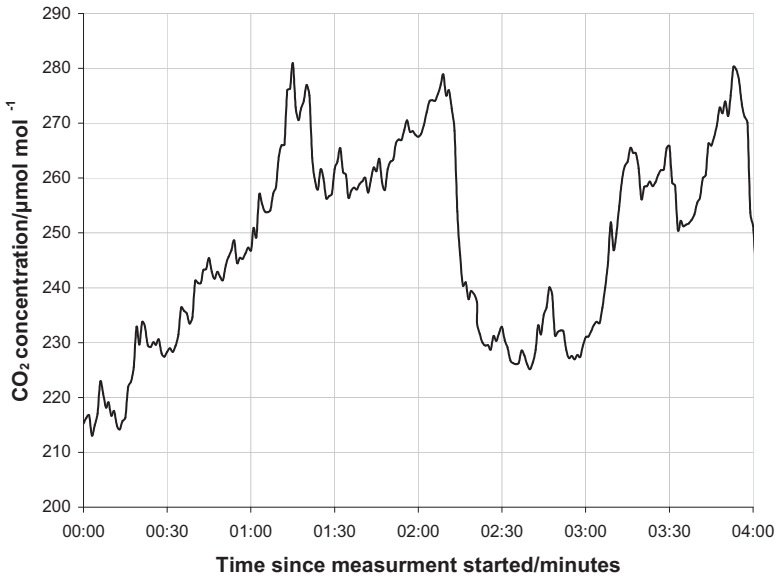

(b)

Figure 2.6: CO_2 concentrations (corrected for water vapour dilution) against time at the same spot on hard ground (a) with collar inserted, and (b) without collar inserted. (a) taken immediately after (b) on the same spot.

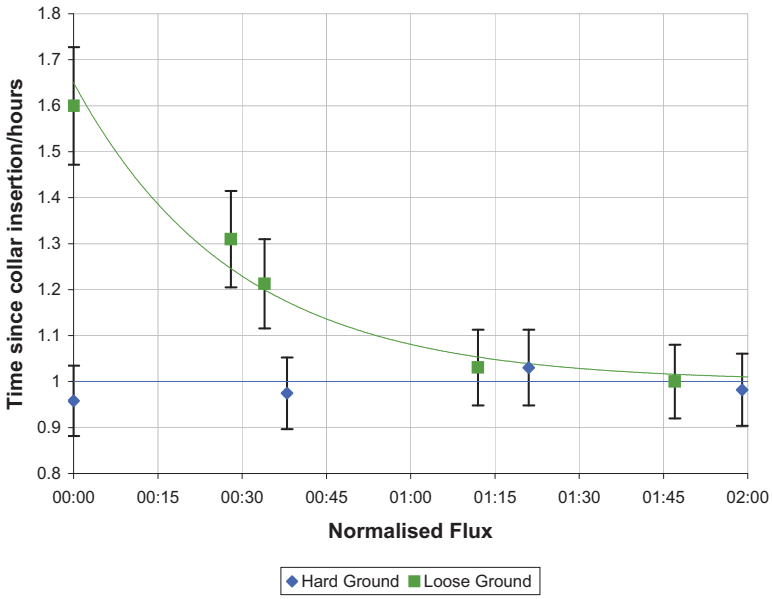

Figure 2.7: Normalised CO_2 fluxes after inserting the collar on hard and loose ground.

of the soil was large enough to soften the PVC collar (figure 2.9). Favara et al. (2001) reported temperatures of up to 90 °C at soil depths of 50 cm. For the rest of the survey, chamber temperatures never varied by more than 3 °C during a measurement, with a mean variation of 0.92 °C.

2.2 Gas Samples

Four samples of volcanic gas were collected, and brought back to Cambridge to be analysed for δ^{13}C. These were collected from Specchio de Venere (figure 1.2). They were collected from bubbles rising through the outskirts of the lake, which made it easy to tell where the source of the emissions were. Collecting samples emerging underwater also prevented contamination with atmospheric gasses.

Samples were trapped with a plastic funnel attached to a copper tube, and stored in the copper tube while in transit (figure 2.10). The other end of the copper tube was inserted into the water, and gas allowed to bubble through

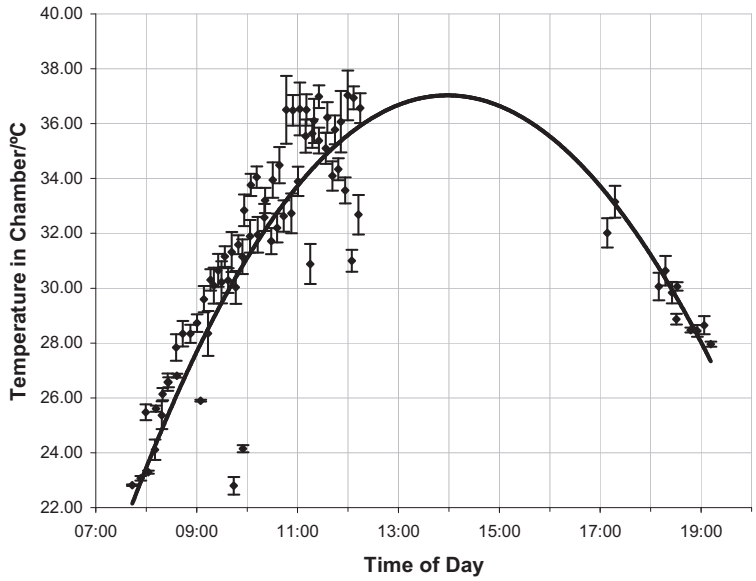

(a) Chamber temperature for measurements taken on 3 September. Error bars represent range of temperatures measured.

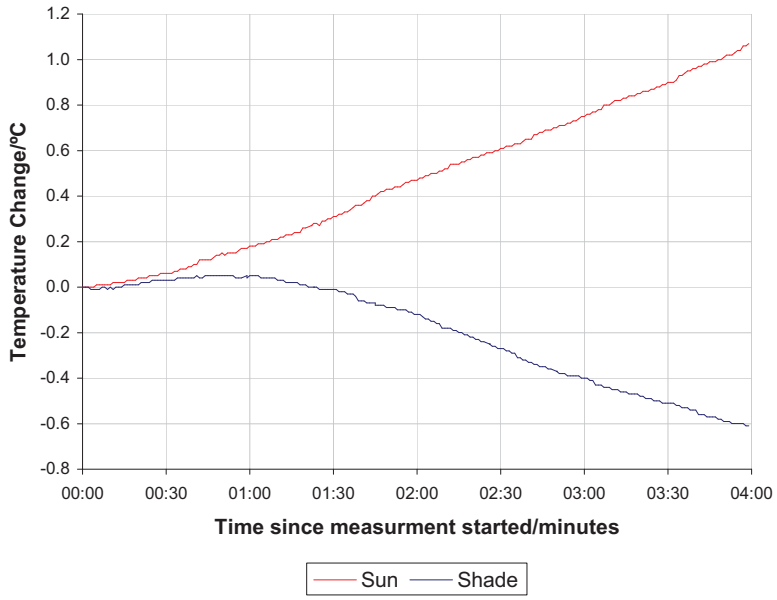

(b) Chamber temperature variation. Measurment 232 and 233, carried out on the same spot, with a CO_2 flux of 50 ± 4 g m^2 d^{-1}

Figure 2.8

Figure 2.9: Plastic collars before (left) and after (right) inserting into the ground in Passo del Vento.

to ensure the tube was flushed out of its previous, atmospheric contents. They were then sealed. An attempt was made to collect samples from the steam vents at Favàra, however the pressure was too low to flush through the pipes.

Back in Cambridge these were dried by freezing. The samples were first cooled to –196 °C using liquid nitrogen, then the noncondensable gasses were removed. The remaining gas was then cooled to –80 °C, so that the water froze but the CO_2 remained as a gas. This was analysed in a Prism dual input mass spectrometer, against a sample of known $\delta^{13}C$. The results were adjusted for the presence of ^{18}O using the method of Craig (1957), with the equations below:

$$\delta^{13}C = 1.0676\ \delta(45/44) - 0.0338\ \delta^{18}O$$

$$\delta^{18}O = 1.0010\ \delta(46/44) - 0.0021\ \delta^{13}C$$

where $\delta(45/44)$ is the ratio of the amount of CO_2 of molecular weight 45

Figure 2.10: Apparatus used to collect gas samples from Specchio de Venere. In the background, to the left, is a bubbling source where gas was collected.

over the amount of CO_2 of molecular weight 44 and $\delta(46/44)$ is similar for molecular weights of 46 over 44. I am grateful to Mike Hall for running these samples.

3. Results

3.1 CO_2 Flux

CO_2 flux readings ranged between 0 – 1900 ± 150 g m^{-2} d^{-1}, with a mean value of 26.8 g m^{-2} d^{-1}. They were distributed approximately log-normally (figure 3.1).

From a log-probability plot (figure 3.2) the background CO_2 flux was estimated to be 3 g m^{-2} d^{-1}, at the first break in slope. There are other breaks in slope above this value, which probably represent different populations relating to different sections of fault.

Contours were created using kriging in ArcMap (figure 3.3). Because kriging works best when the underlying distribution is normal (Haining, 2003), logged values were used for the contour creation. Values were then converted back into g m^{-2} d^{-1}.

From the kriging model, the total CO_2 flux is 1 380 kg d^{-1}, over an area of 0.163 km^2. Summing only those areas above the background flux of 3 g m−2 d^{-1}, we get a total flux of 1 300 kg d^{-1} over an area of 0.084 km^2. This works out as 475 T yr^{-1}, at an average of 16 g m^{-2} d^{-1}. This is lower than the mean value of the sample sites: 26.8 g m^{-1} d^{-1}. This discrepancy is probably due to the greater sampling density over the areas of high flux (figure 3.4).

Semivariograms are used in the kriging process. Figure 3.5 shows the semivariograms for two perpendicular directions. The difference squared between pairs of points (averaged for a given separation), γ, is plotted against the separation, or lag distance. The more spatially dependant or autocorrelated the data is, the shallower the gradient of the semivariogram model. From figure 3.5, it is clear that the spatial dependence of the CO_2 flux is anisotropic. The direction of the highest autocorrelation is shown by the semivariogram surface — which plots γ at different lag distances and angles — to be 029° (figure 3.6).

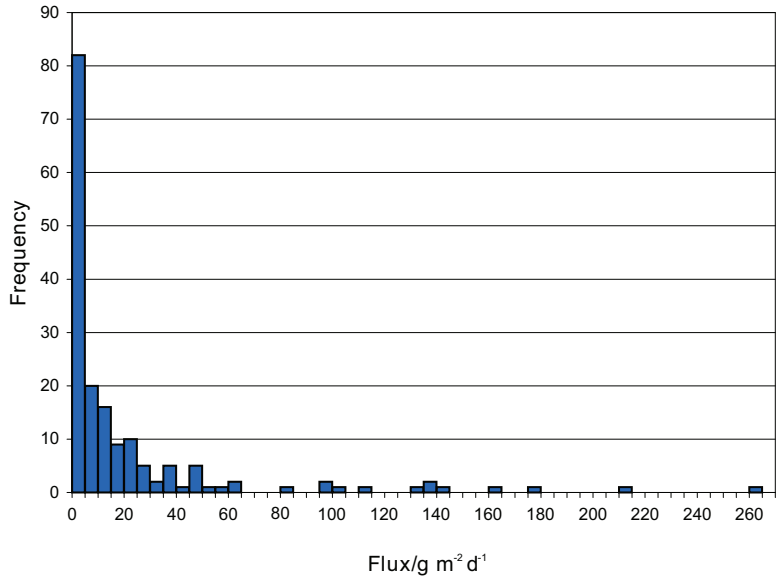

(a)

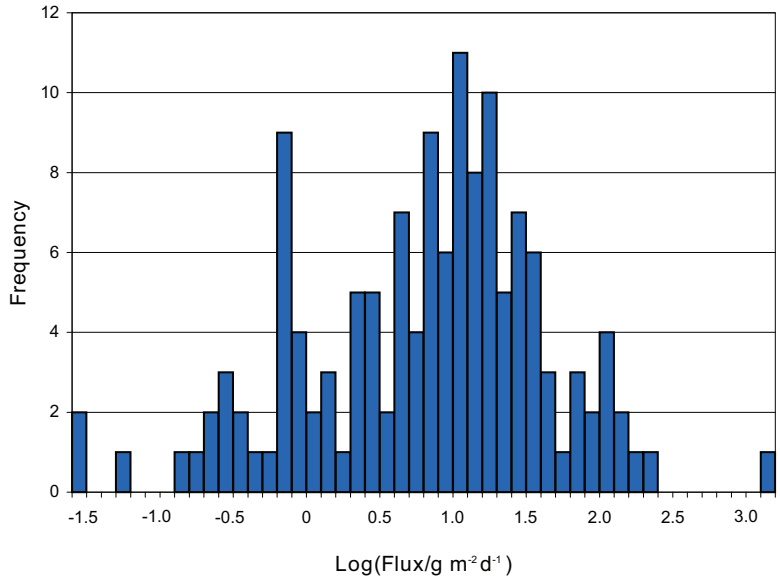

(b)

Figure 3.1: Histograms of (a) the CO_2 flux readings and (b) the log of the CO_2 flux readings. The peak in the logged values is equivalent to 13 g m^{-2} d^{-1}

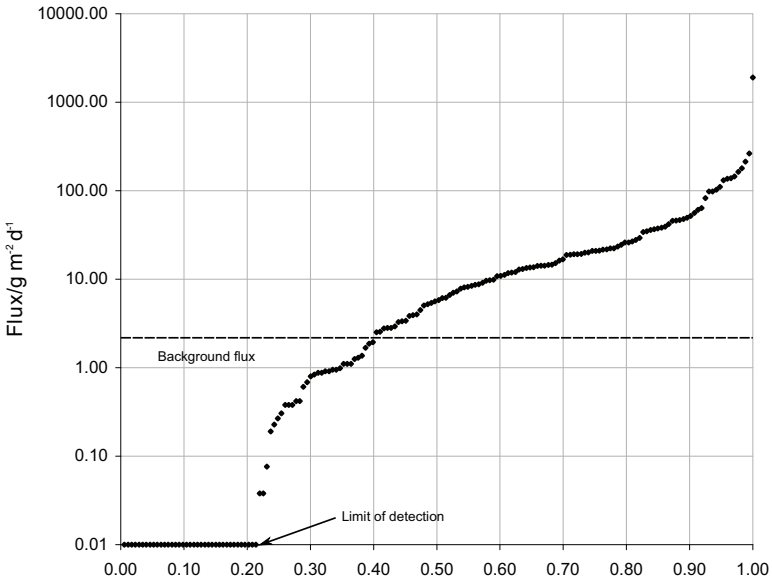

Figure 3.2: Log-probability plot for the CO_2 flux readings. The first break in slope is at 3 g m^{-2} d^{-1}, and this is assumed to be the background flux

In figure 3.5, the autocorrelation does not reach zero at zero separation distance. The intercept point on the y-axis is know as the nugget, and is a function of both the measurement error and variation at scales below the resolution of the survey. The nugget here is 0.74, which is equivalent to 21 g m^{-2} d^{-1}. Assuming the measurement error is 8%, then the average measurement error is 2.1 g m^{-2} d^{-1}. This shows that there is some variation at smaller scales than was measured. This is also apparent in figure 3.7, which shows that there was variation on a scale of a couple of meters. Figure 3.8 also shows that kriging underestimates the variation of the flux. This is particularlly accute at high fluxes. While there were 19 flux measurements made above 100 g m^{-2} d^{-1}, none of the kriged values were this high. In order to compensate for the small scale of the highest fluxes, sample sites were spaced more closely near areas of high flux (figure 3.4). In order to map the anomalies in greater detail, less of an area would have been covered. CO_2 from fumeroles was also neglected because the equipment couldn't measure this.

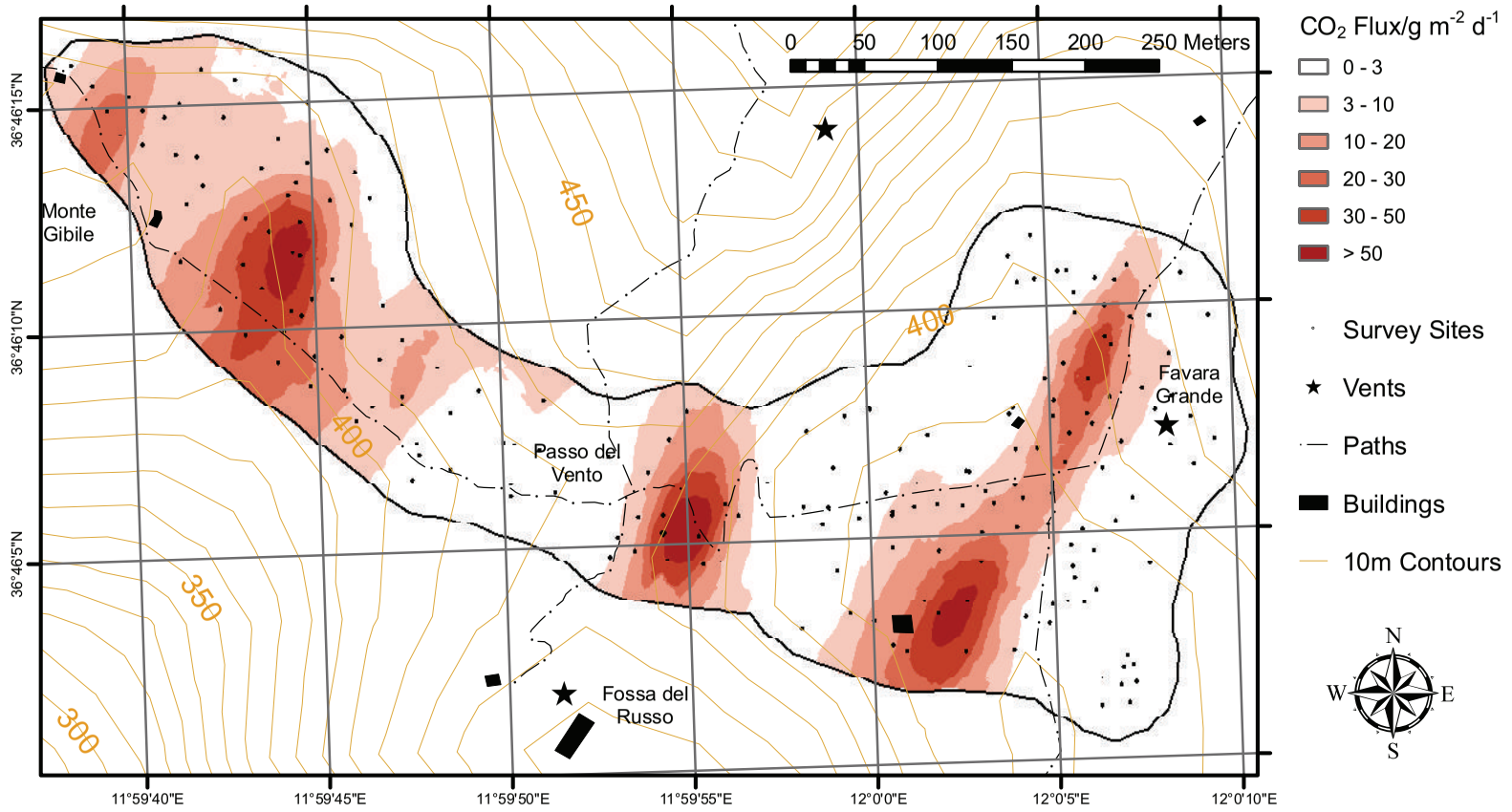

Figure 3.3: Results of the CO_2 flux survey. Coloured areas represent places where the flux was higher than background flux of 3 g m^{-2} d^{-1}.

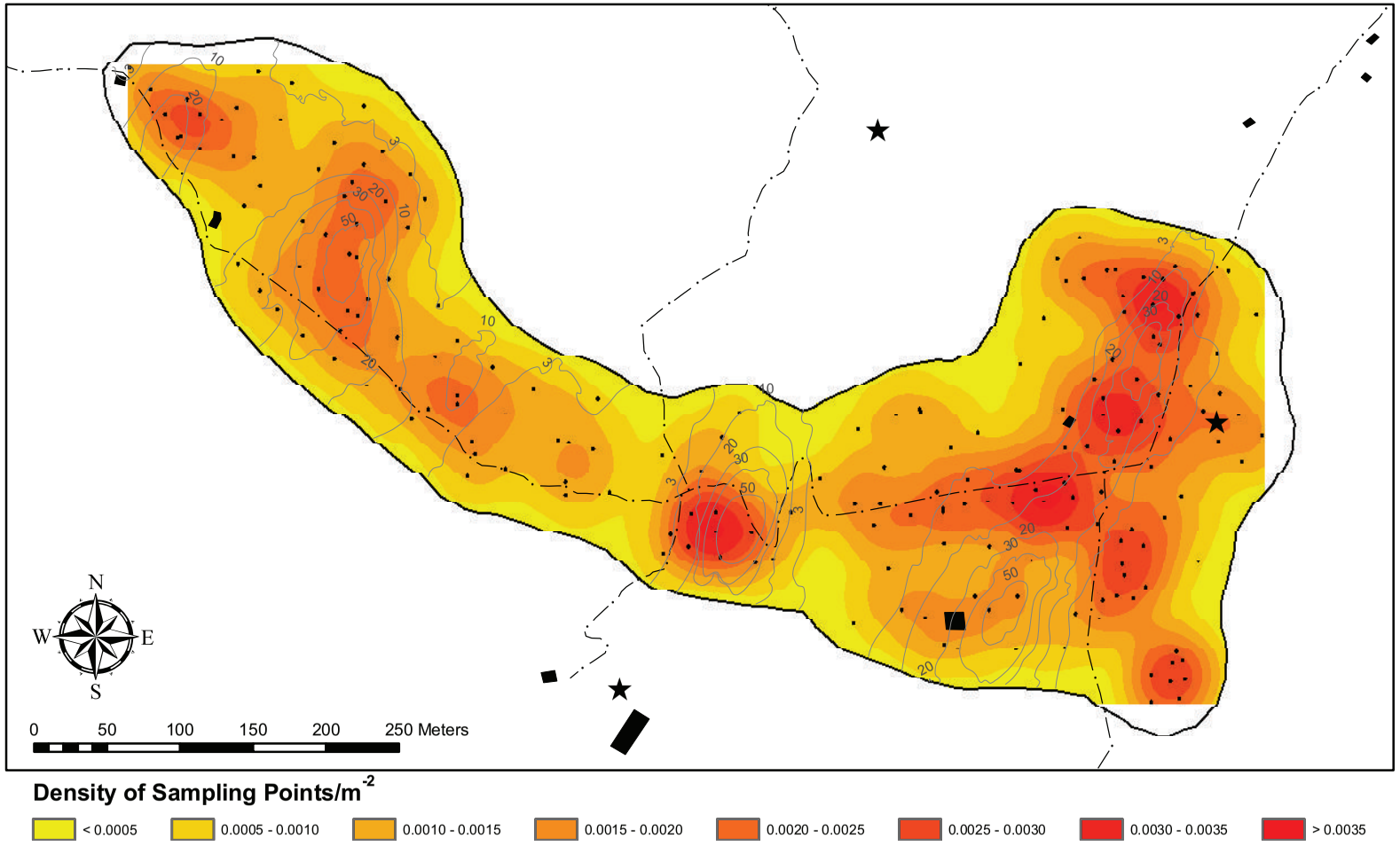

Figure 3.4: Density of sampling points. The average density was 0.0014 m^{-2}, which equates to a spacing of 27 m between points. The grey lines are contours of the CO_2 flux.

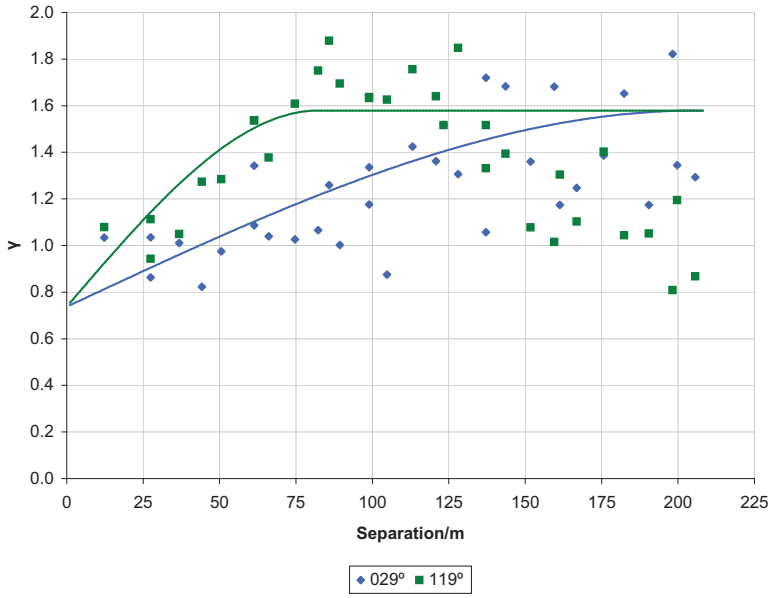

Figure 3.5: Semivariograms of the CO_2 flux for two perpendicular directions. γ is in $\log(\mu\text{mol m}^{-2}\text{ s}^{-1})$.

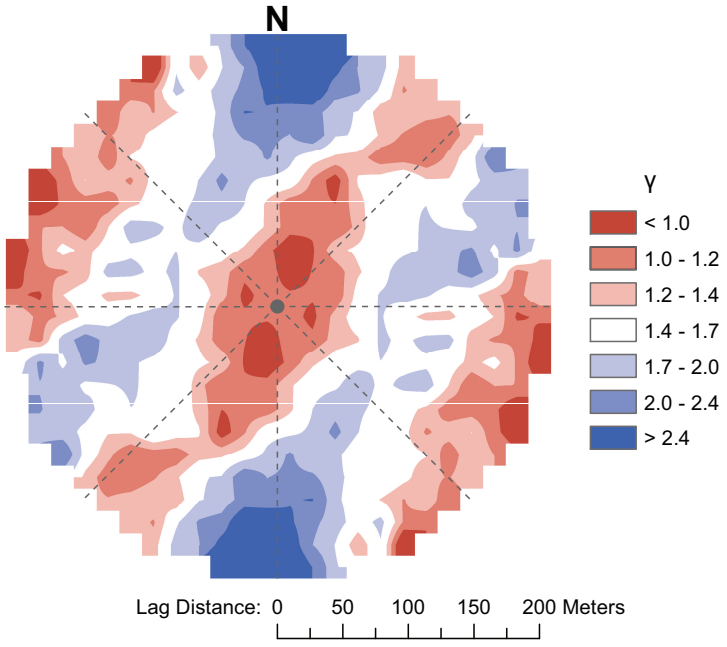

Figure 3.6: Semivariogram surface for the CO_2 flux. γ is in $\log(\mu\text{mol m}^{-2}\text{ s}^{-1})$. Lag distance is the distance between points that γ is calculated for.

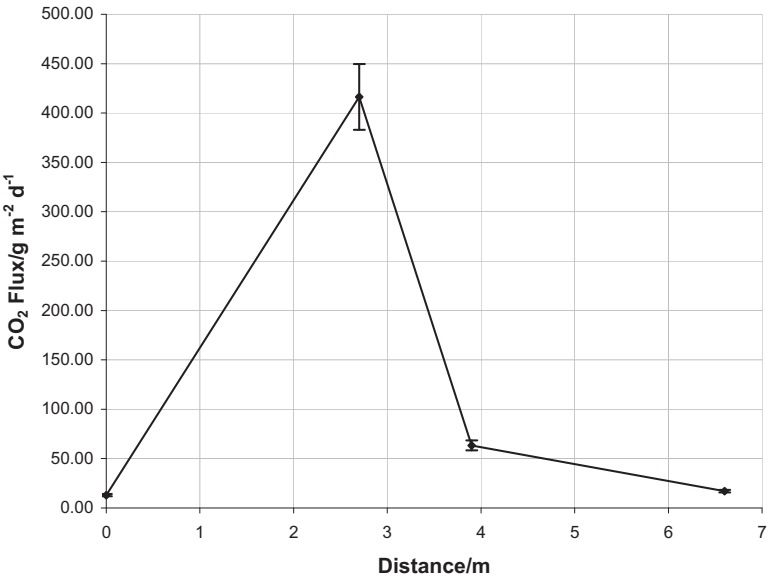

Figure 3.7: Results of a small scale survey done in a straight line over an area of high CO_2 flux.

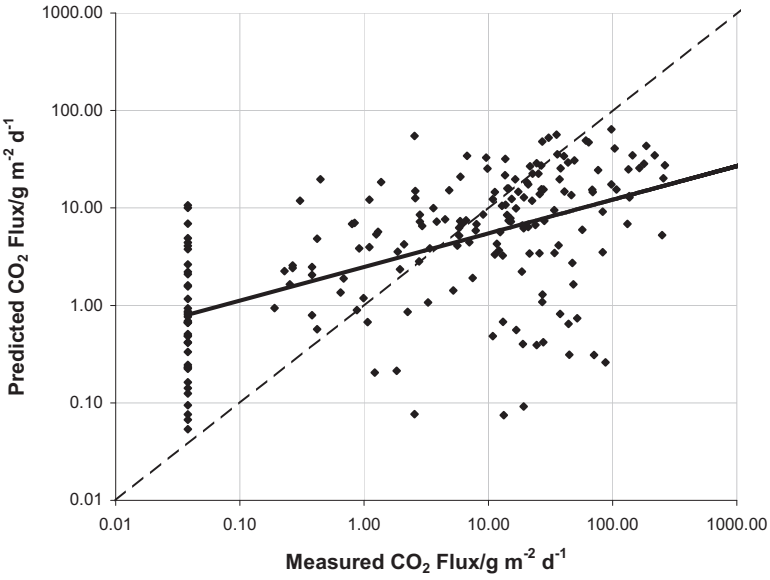

Figure 3.8: Measured CO_2 flux against flux predicted from the kriging model.

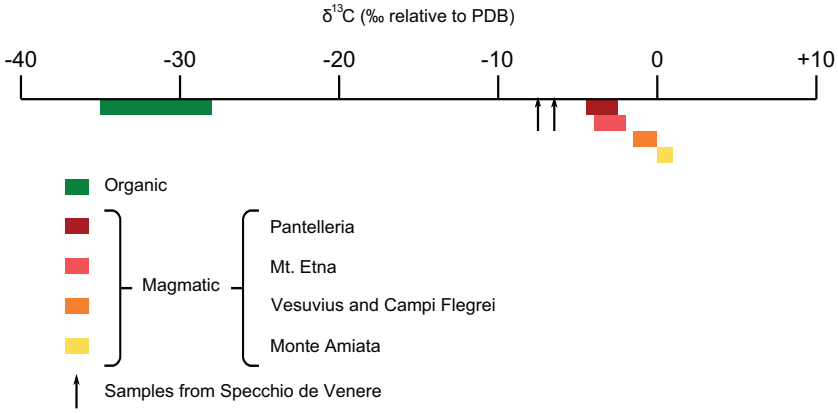

Figure 3.9: δ^{13}C isotopic data. For sample sites, see page 9. Magmatic δ^{13}C values from Parello et al. (2000).

3.2 δ^{13}C Isotope Data

Results for the δ^{13}C are shown in figure 3.9. One of the four sample leaked before it could be analysed. Another didn't contain any CO_2, but this was taken from a source with a low flow rate and probably didn't have enough pressure to flush the tube through. The δ^{13}C for the remaining two samples was –7.55 ‰ and –6.45 ‰, relative to PDB. This is close to the mantle value of –4 ‰ (Parello et al., 2000), and shows that 80–90 % of the gas is magmatic in orign.

4. Discussion

4.1 Comparison With Previous Work

The annual value here is smaller than the value of 13 000 T yr^{-1} reported by Favara et al. (2001) for a 1998 survey. It is also smaller than the 2 100 T yr^{-1} found by D'Alessandro (2007) in 2005. This suggests the CO_2 flux may be decreasing in time, and when graphed this decrease appears exponential (figure 4.1). Exponential regression suggest a time constant — the time it takes for the flux to decrease by a factor of e — of 3.4 years. This would be expected if the gas is from fresh magma injected in discreet batches: as the magma becomes less gas-rich it will degas slower.

However, the large estimate by Favara et al. is probably an overestimate due to the low sampling density: only 20 measurements were made around Favàra Grande. Kriging generally overestimates quantities when the spatial resolution is low. Meteorological conditions have a large impact on the CO_2 flux measured at the surface. An increase of 70 % was measured over a period of a week in this survey, although this would only increase the total flux measured in this survey to 800 T yr^{-1} and so is not large enough to explain the change. Differences in the areas measured also may contribute to these apparent decreases. Even if the differences between these surveys are real, they may not represent a decreasing trend. Only three data points do not allow firm conclusions to be drawn, and the trend may simply be random variation.

4.2 Relationship Between CO_2 Flux and the Geology

Figure 4.2 shows that the bulk of the anomalous degassing occurs along linear features that run through the area. From the semivariogram surface (figure

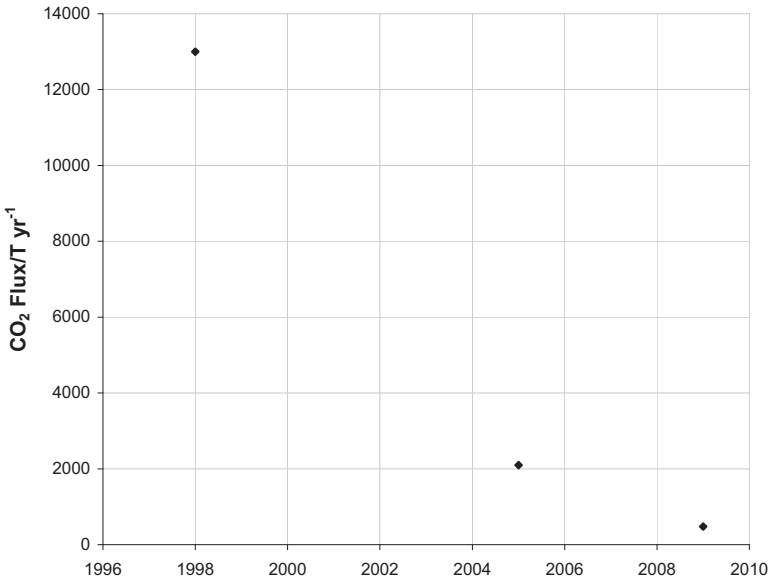

Figure 4.1: Results of three surveys of CO_2 flux around Favàra Grande. 1998 survey is from Favara et al. (2001), 2005 survey is from D'Alessandro (2007), 2009 is this study.

3.6), the direction of highest autocorrelation is about 029°. This is similar to the direction that the faults run in, suggesting that this is what is controlling the spatial variation of the flux.

The faults shown are slightly modified from Mahood and Hildreth (1986). Aerial photos were used to draw them where they outcropped (figure 1.5), but where they were covered the CO_2 flux could be used to draw them in.

Areas of high CO_2 flux have high methane fluxes (D'Alessandro et al., 2009). Methane is also associated with magmatic degassing.

Areas of high flux were often associated with altered bedrock (figure 4.2, 4.3). The predominantly grey trachytes and pantellerites became green and orange, and friable. Around some of the vents the rock was altered to a red clay, and there was also some calcareous and sulphur mineralisation around areas of high flux (figure 4.4, 4.5). From this it is possible to imply that areas of altered bedrock that were not surveyed would likely be areas of degassing, some of which are shown on figure 4.2. The area between Montagna Grande

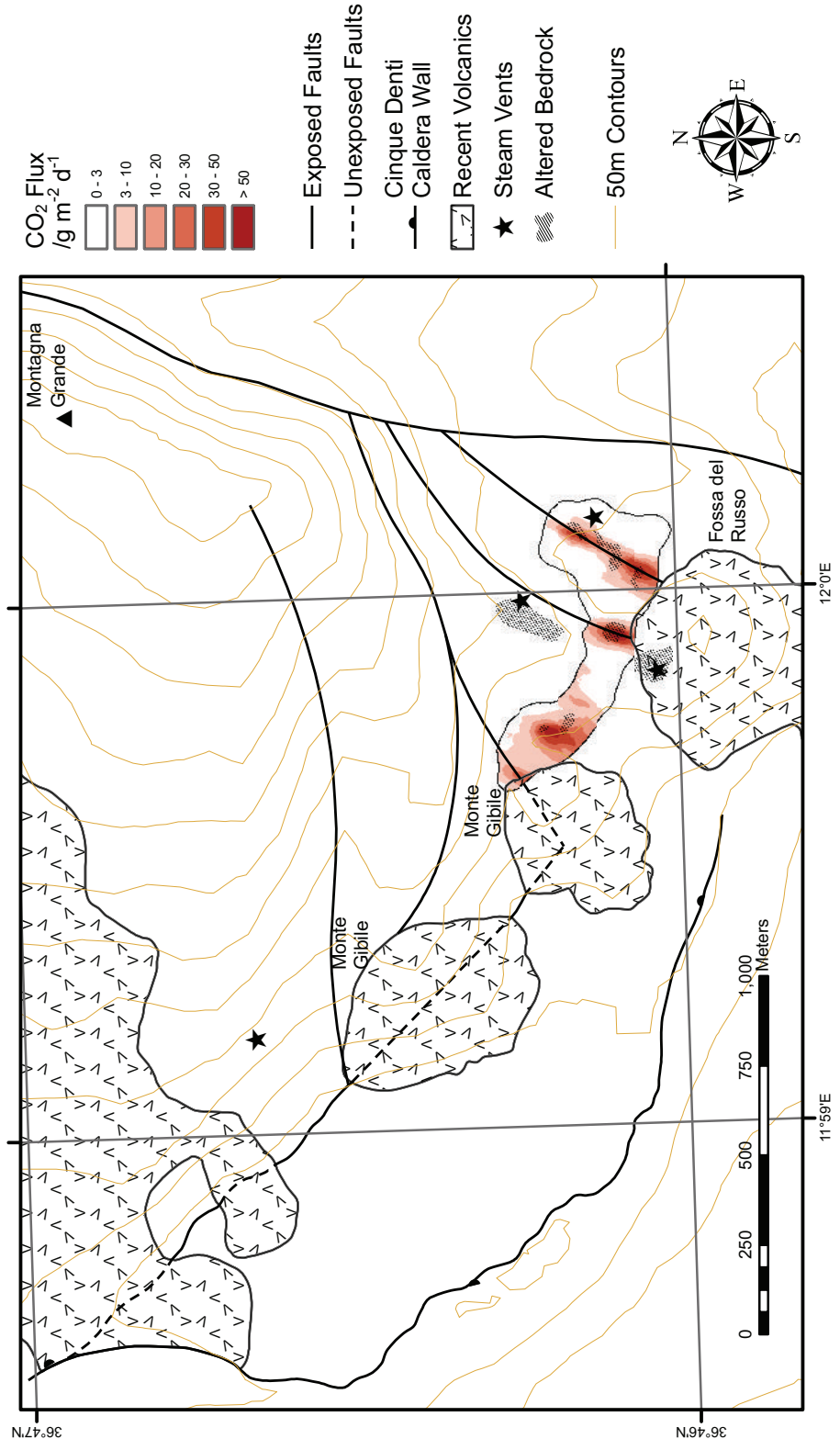

Figure 4.2: CO_2 flux overlain on a sketch map of the geology, modified from Mahood and Hildreth (1986).

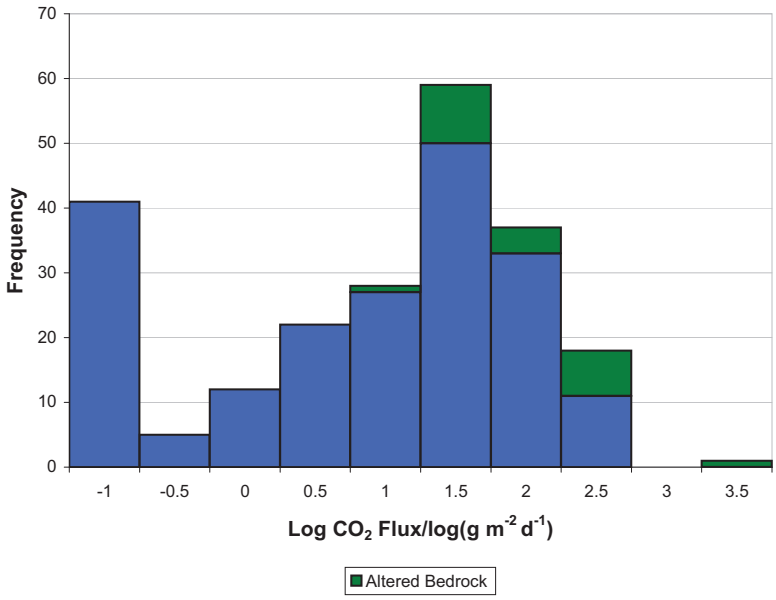

Figure 4.3: Histogram of flux measurements. Green bars show measurements where altered bedrock was visible at the surface.

and Monte Gibele also had altered bedrock, suggesting that the Montagna Grande Fault has at least in the past been a pathway for degassing.

Faults are likely to be a pathway for degassing as they have increased permeability. Unfractured rocks, especially crystalline volcanic rocks, are very impermeable. Faulting fractures the rock, increasing the permeability.This suggests that these faults may be active, as permeability can be decreased by mineralisation along inactive faults. These could be taking up some of the deformation acting on the island.

The permeability, κ, of the faults can be estimated from the CO_2 flux using Darcy's law:

$$\kappa = -\frac{\mu Q \Delta z}{A \Delta p}$$

where μ is the dynamic viscosity of CO_2; Q is the volume flux of CO_2; Δz is the distance over which the CO_2 flows; A is the cross-sectional area of the channel which the CO_2 flows along; and Δp is the pressure gradient acting on the CO_2.

Figure 4.4: Costa della Favàra, taken from just above Favàra Grande, showing the relationship between faulting, mineralisation and steam vents.

(a) Red clay and sulphur deposits around area of steaming ground in Passo del Vento. Camera case is ∼10 cm long.

(b) Mineralisation around area of high flux in the centre of Costa Favàra. Notebook is ∼15 × 20 cm.

Figure 4.5

The dynamic viscosity of CO_2 varies depending on temperature, from 3.9×10^{-5} N s m^{-2} at 700 °C in the magma chamber to 1.5×10^{-5} N s m^{-2} at 30 °C at the surface. An intermediate value of 2.5×10^{-5} N s m^{-2} is used in this calculation. The flux of CO_2 over the area measured is 0.34 mol s^{-1}, however the volume depends on the temperature and pressure. Under magma chamber conditions 0.34 moles of CO_2 takes up 28 cm^3 of volume, but at the surface this expands to 9 250 cm^3. An intermediate value of 5 000 cm^3 is used for this calculation. Δz and Δp are estimated assuming the gas come from the top of the magma chamber at lithostatic pressure. Δz is therefore 3.5 km, and Δp 100 MPa. The cross-sectional area of flow is the hardest to estimate. The area of anomalous degassing is 83 600 m^2, however much of this is probably due to lateral diffusion in the soil at the surface. The highest fluxes are concentrated in much smaller areas, and the total area of the faults transporting the CO_2 to the surface is likely to be of the order of 1–10 m^2. Using these numbers, the permeability is 10^{-8}–10^{-9} cm^2, which is typical of fractured igneous rocks (Bredehoeft and Norton, 1990). Unfractured igneous rocks typically have a permeability of 10^{-13}–10^{-17} cm^2.

4.3 Deformation Data

Before 1979 deformation data is sparse. Butler (1892) reported 80 cm of uplift along the northeast coast of the island in the two years preceding the 1891 eruption. Several paleo-shorelines have been found along this coast, dated using ^{14}C from corals and vermatids at ∼100, ∼500 and ∼900 years before present (de Guidi and Monaco, 2009). These were uplifted ∼1.1 m, ∼3.2 m and ∼4.8 m respectively. There are overlaps between the dates of fossils found at the different paleo-shorelines, therefore the uplift must have been rapid, occurring faster than the resolution of ^{14}C dating (a few decades). The 1891 event was associated with an eruption, but there are no historical records of eruptions ∼500 and ∼900 years ago. There are some undated basic cones in the northwest of the island that could could be related, or there could have been a sub-marine eruption.

Since 1979 several surveys have been undertaken to quantify current

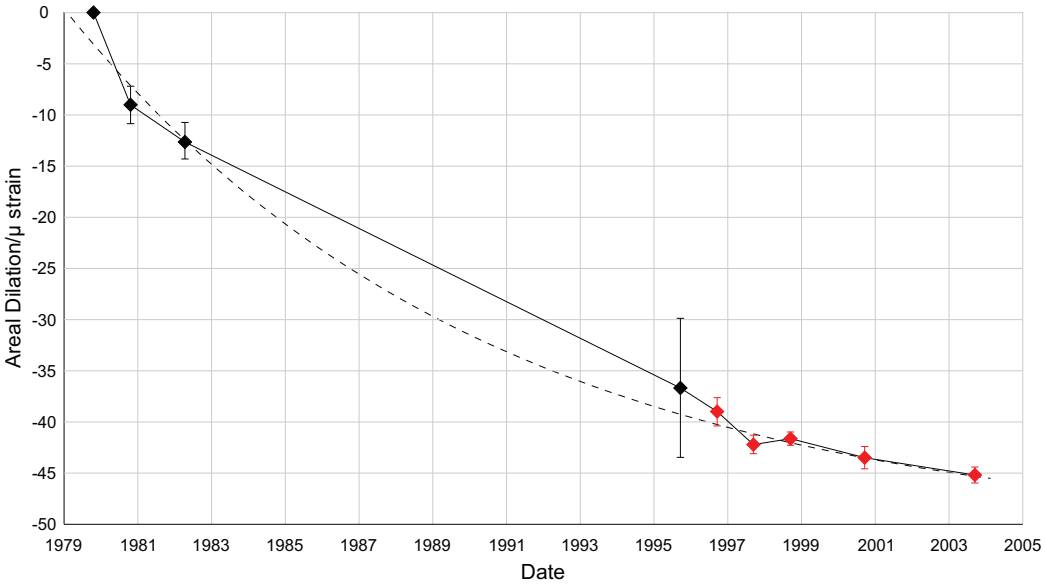

(a)

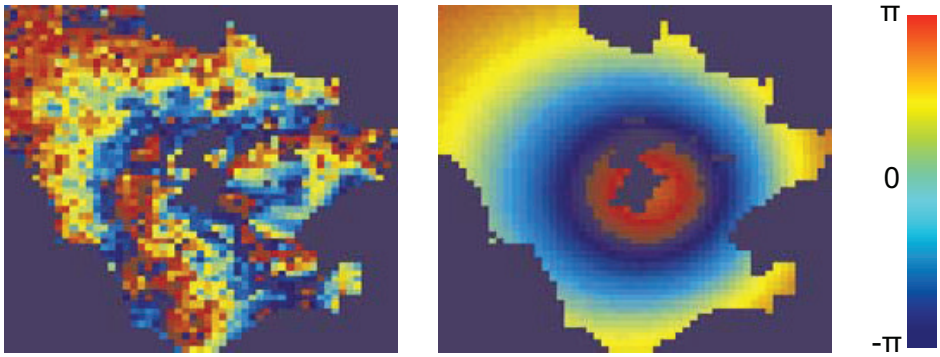

(b) (c)

Figure 4.6: (a) Areal dilation acting on Pantelleria over the last 30 years. Red symbols indicate GPS readings, dashed line is an exponential regression. (b) InSAR data between 15 August 1995 and 2 March 1999. (c) Modelled InSAR data, assuming a Mogi point source. Modified from Mattia et al. (2007)

ground deformation on the island (Behncke et al., 2006; Bonaccorso and Mattia, 2000; Mattia et al., 2007; Obrizzo et al., 1993). Mattia et al. provide the most up-to-date summery of the collected data, including: levelling lines; electro-optical distance meter (EDM) measurements; GPS measurements; and differential interferometry synthetic aperture radar (DInSAR) data. They used this data to model the deformation using a Mogi point source, obtaining a best fit for a depth of 4 456 m with respect to a reference height of 400 m, and with a annual change in volume of –0.84 $\times$ 10^6 m^3 (figure 4.6). This matches with petrological results suggesting the top of the magma chamber is $\leq$ 3.6 km deep (Gioncada and Landi, 2010). Although Mattia et al. assumed a constant rate of deflation in order to calculate the magma chamber parameters, the rate of areal dilation appears to be slowing with time. An exponential regression fits well, with a time constant — the time taken for the dilation rate to decrease by a factor of e — of about 11 years. If the degassing rate is slowing, and the deformation is caused by the degassing, then the rate of deflation would also be slowing. The time constant for deflation is longer than that calculated for degassing, although if the relationship between source volume change and surface areal dilation is not linear then this would be expected.

There are three main possible causes of the deflation: volatile degassing; changes in the hydrothermal system and thermal contraction (figure 4.7). These are discussed below. The inflationary events could be caused by the injection of fresh magma into a magma chamber or hydrothermal activity.

4.3.1 Volatile Degassing

Volatiles exsolve from the magma as the pressure drops, forming bubbles. These rise through the melt to the top of the chamber, and often escape through fractures in the overlying rock. This lowers the volume of the magma chamber, which could cause the deflation seen at the surface. The major volatiles found in Pantellerian magmas are water and CO_2. Most of the water will remain in solution until the magma reaches very shallow depths, while CO_2 is far less soluble (figure 4.8(a)). CO_2 will be the only significant

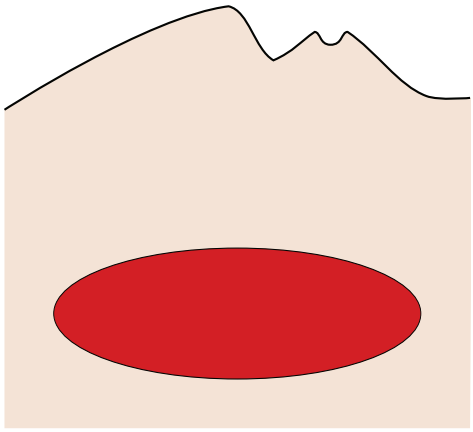

(a) Pre-deflation Pantelleria.

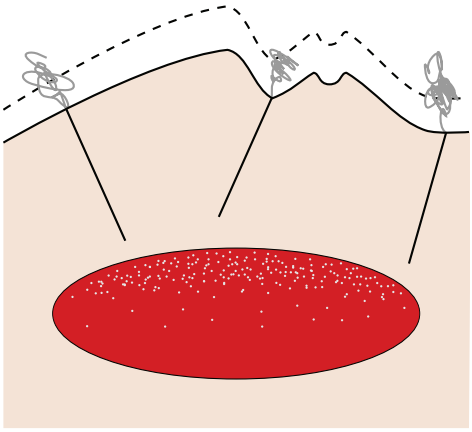

(b) Volatiles escaping from the magma through fractures, reducing the volume of the magma chamber.

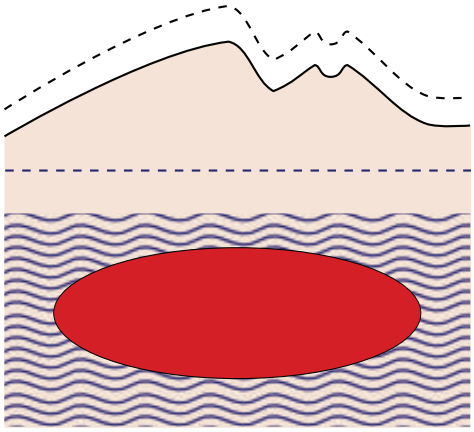

(c) Lowering of the water table in the hydrothermal system causing deflation.

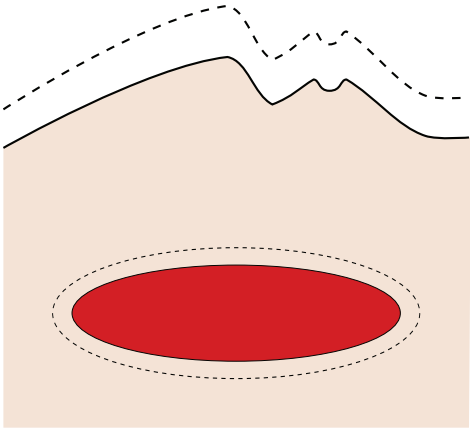

(d) Contraction of the magma chamber due to thermal effects.

Figure 4.7: Cartoons representing possible causes of the deflation acting on Pantelleria.

volatile phase in the magma chamber.

Using the ideal gas laws, we can calculate the volume, V, of CO_2 at magma chamber pressures and temperatures using the following equation:

$$V = \frac{nRT}{p}$$

where n is the number of moles; R is the gas constant (8.31 J K^{-1} mol^{-1}); T is the temperature (K); and p is the pressure (Pa). Assuming the magma chamber is 700 °C and at 4.5 km depth (White et al., 2009 and Mattia et al., 2007 respectively), then the 475 T yr^{-1} measured in this survey would be 690 m^3 in volume.

This is much lower than the 0.84 × 10^6 m^3 calculated by Mattia et al.. Favara et al. (2001) estimated the total CO_2 flux from the island, including CO_2 dissolve in water, at 0.39 MT yr^{-1}. If this amount escaped the chamber, it would contract by 0.57 × 10^6 m^3. This is still lower than calculated by Mattia et al., and may well be an overestimate due to the low sampling density. The majority of this value (0.32 MT yr^{-1}) comes from diffuse soil measured using an island-wide survey with about 1 point per km^2. Of these 91 points, only five were considered above the organic CO_2 threshold and used to calculate the total. Each of these anomalous values was assumed to be representative of 1 km^2, and these were summed. From this survey it is clear that most of the anomalous degassing occurs along small features, and the total area of anomalous degassing in this survey was 0.084 km^2. Their value for the flux around Favàra Grande is also much higher than measured here: 13 000 T yr−1 compared to 475 T yr^{-1}. This may be due to undersampling, or it may be due to a real change in the CO_2 output of the island. Either way, it is unlikely that the current CO_2 flux from the island is 0.39 MT yr^{-1}. In order to fully explain the deformation seen at the surface, 0.58 MT yr^{-1} of CO_2 needs to escape the chamber. While it is possible that some CO_2 escapes to the surface without being measured, it is unlikely that this much could remain hidden.

The amount of CO_2 bubbles in the magma chamber is a function of the solubility of CO_2, the initial concentration in the magma and the depth of

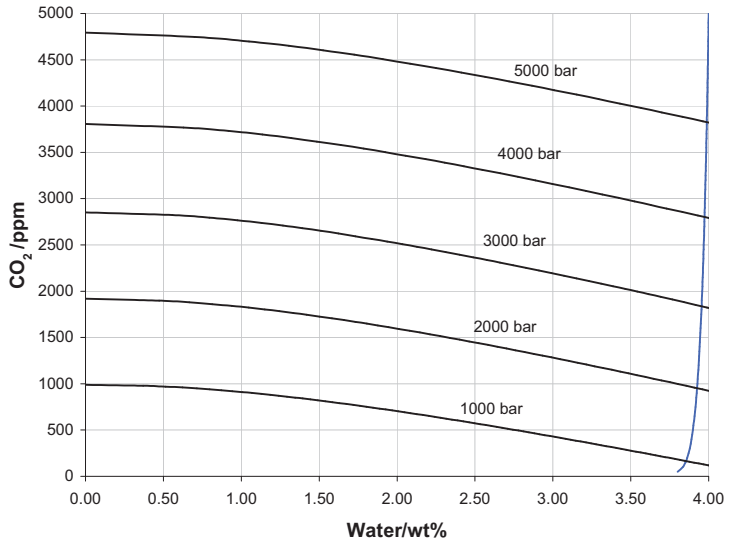

(a)

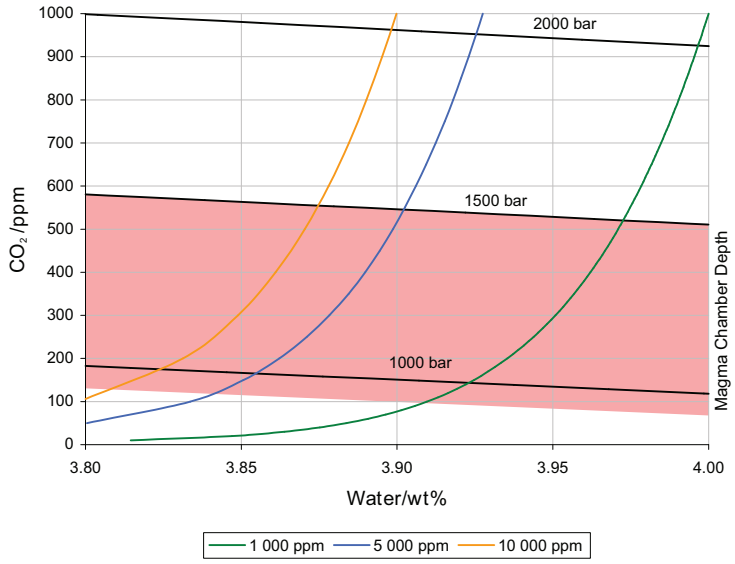

(b)

Figure 4.8: Degassing paths for rhyolitic magma at 700 °C. (a) is for an initial concentration of 5 000 ppm CO_2 and 4 wt% water. (b) shows the path over the range of pressures representing the magma chamber. The initial water concentration in each case is 4 wt%, while the initial CO_2 concentration is shown by the different colours. Calculated using VolatileCalc 1.1 (Newman and Lowenstern, 2002).

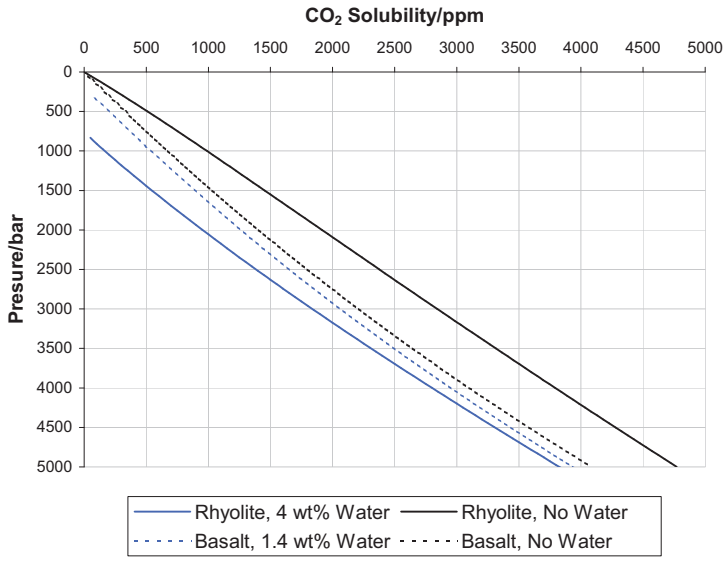

Figure 4.9: Solubility curves for CO_2 in a rhyolitic melt at 700 °C and a basaltic melt at 1100 °C. Water content and temperatures taken from White et al. (2009) and Gioncada and Landi (2010) for rhyolite and basalt respectively. Calculated using VolatileCalc 1.1 (Newman and Lowenstern, 2002).

the magma chamber. Solubility curves are shown in figure 4.9 for rhyolite and basalt. The high peralkalinity of Pantellerian rhyolites may affect the solubility of CO_2, however these calculations should provide a good approximation of the true values. Dissolved water in the melt lowers the solubility of CO_2, while fractionation from basalt to rhyolite increases it. However, Pantellerian pantellerites are more water-rich than the basalts (Gioncada and Landi, 2010), making CO_2 less soluble in the pantellerites.

The initial CO_2 content of the magma is much harder to pin down. Naumov et al. (1989) and Lowenstern (1994) found bubbles of pure CO_2 in melt inclusions, however the dissolved CO_2 in the melt inclusion itself was below the level of detection (100 ppm). From figure 4.9, this level is reached at a pressure of 1000 bar, or at just over 3 km depth. As the centre of the magma chamber is only at $\sim$ 4.5 km depth it is very likely that almost all the CO_2 would have exsolved before melt inclusions became trapped.

Gioncada and Landi (2010) measured up to 980 ppm CO_2 in melt inclu-

sions in a basalt from the northwest of the island. These basalts are thought to be representative of the magmas feeding the pantelleritic magma chamber, so their CO_2 content shows how much CO_2 will have exsolved during ascent and fractionation. However, Gioncada and Landi suggest that the basalts ponded at about 7 km depth, where the 980 ppm CO_2 represents a saturated melt (figure 4.9). This means that 980 ppm is a lower bound on the initial CO_2 concentration, as basalts entering the shallow chamber may have greater CO_2 concentrations. They also found CO_2 concentrations in melt inclusions from pantellerites was below the limit of detection, consistent with them residing in a shallow chamber.

Figure 4.8 shows the path taken by degassing volatiles for several different initial concentrations of CO_2. From these we can calculate the amount of CO_2 that would have exsolved by the time the magma reached a depth of 4.5 km. For an initial concentration of 5 000 ppm, 11 kg of CO_2 would be exsolved for every cubic metre of magma [assuming the density of pantelleritic magma is 2 425 kg m−3 (D. Neave, personal communication). At magma chamber pressures and temperatures this would occupy 0.016 m^3. In order to produce the surface deformation observed, 53×10^6 m^3 of magma would have to degas every year. Civetta et al. (1988) estimated the long-term resupply rate for the magma chamber beneath Pantelleria at 1×10^6 m^3 yr^{-1} from eruption and chemical differentiation rates. Even with an initial CO_2 concentration of 10 000 ppm, 25×10^6 m^3 yr^{-1} of magma is required to degas. For the ∼1 000 ppm found in basalts by Gioncada and Landi, this rises to 385×10^6 m^3 yr^{-1}.

If the resupply rate calculated by Civetta et al. is correct, the initial CO_2 concentration would have to be unrealistically high. However, the current degassing rate may not be representative of the long-term degassing rate. A fresh injection of magma would contain more CO_2 and would degas faster than the average rate, slowing as the CO_2 concentration dropped. A recent injection would explain the high degassing rate while remaining consistent with the long-term re-supply rate.

There was likely an injection of fresh magma before the 1891 eruption, causing the uplifted coast and triggering the eruption. It is not clear whether

any magma entered the chamber below Montagna Grande, as the erupted products were basic while magma erupted from the chamber is rhyolitic. A basic calculation shows that an injection and complete degassing of 20–40 $\times$ 10^6 m^3 of fresh magma between 1975 and 1985 is both consistent with the long term trend in degassing hypothesised above and the suggested long term recharge rate of 1 $\times$ 10^6 m^3 yr^{-1}. There are, however, large uncertainties in the long-term degassing rate. There is also no evidence of any uplift associated with and injection of magma at this time, although geodetic measurements only started in 1979.

4.3.2 Hydrothermal Activity

Changes in the pattern of hydrothermal circulation around the chamber can affect the level of the water table. Lower water tables could lead to deflation on the surface.

There is an active hydrothermal system acting on Pantelleria, centred on the southern part of Montagna Grande (Squarci et al., 1994). At the bottom of well PT3 (300m depth), southeast of Favàra (figure 4.10), temperatures reach 140 °C and the gradient is ∼140 °C km^{-1}, and Gianelli and Grassi (2001) drilled a deeper hole nearby, and found temperatures of 240 °C at a depth of ∼2 km. The geothermal system is recharged both from meteoric and sea water.

Bradyseism, or uplift and deflation events, have been recorded at Campi Flegrei, near Naples. This has been attributed to hydrothermal activity (Lima et al., 2009). Water released from the magma chamber, either due to a fresh input of magma or due to a cyclical build-up of pressure being released, fills fissures above the chamber. Rapid uplift is followed by a slower deflation, as the system returns to equilibrium. The size of the uplift at Campi Flegrei is similar to that recorded by the paleo-shorelines on Pantelleria (1–2 m), so could explain the past uplift on Pantelleria. The deflation over the past 30 years is harder to explain with hydrothermal activity. The time-scale of the events at Campi Flegrei is 1–10 years, much shorter than the time-scales at Pantelleria. Also, at Campi Flegrei the magma chamber is deeper (∼6 km),

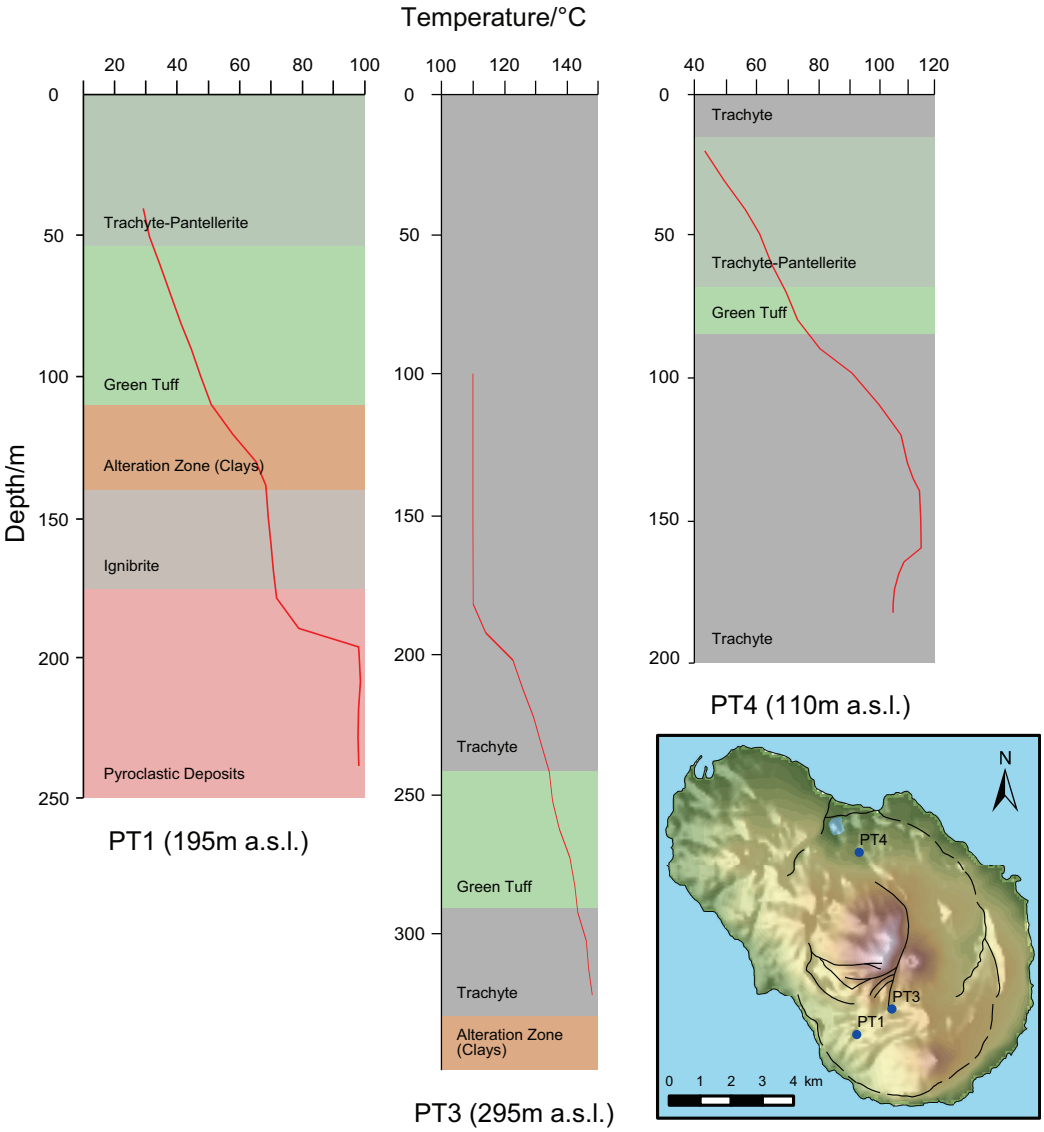

Figure 4.10: Well data taken from Squarci et al. (1994), showing the elevated temperatures of water below Pantelleria.

Table 4.1: Cooling rates for some magma chambers. (1) Kuritani et al. (2007), (2) Scheibner et al. (2008), (3) Tomiya and Takahashi (1995), (4) Turner et al. (2003) (5) Cooper et al. (2001).

	Magma Chamber				
Volcano	Volume /km^3	Depth /km	Temperature /°C	Cooling Rate /°C yr^{-1}	
Rishiri, Japan	280	7	1100–940	>0.1	(1)
Vesuvius, Italy	9	7–8	900–775	0.024	(2)
Usu, Japan	6	> 3	880–790	0.85	(3)
Sangeang Api, Indonesia	6–10	< 30	1000	0.05	(4)
Kilauea, Hawaii	2–3	2–4	1350–1150	0.1	(5)

an the surface deformation is caused by magmatic fluids at similar depths to the Pantellerian magma chamber.

4.3.3 Thermal Contraction

Thermal contraction happens to all materials as they cool. There is a trade-off between the volume of the magma chamber and the change in temperature, however some estimates as to the likely magnitude of the effect in Pantelleria can still be obtained. The equation for thermal contraction is:

$$\frac{\Delta V}{V} = \alpha_v \Delta T$$

where ΔV is the change in volume; V is the total volume; α_v is the volumetric thermal expansion coefficient; and ΔT is the change in temperature. Using 3×10^{-3} K^{-1} as the volumetric thermal expansion coefficient (measured by Bagdassarov et al. (1996) for peralkaline rhyolite at 600 °C) the relationship between the total volume of the magma chamber in cubic meters and the yearly change in temperature in degrees celsius is:

$$V = \frac{280 \times 10^6}{\Delta T}$$

Assuming a volume of 30 km^3 for the magma chamber, the temperature

change required to explain the deflation is 0.001 K yr^{-1}. This is lower than many other volcanic systems (table 4.1), however volatile exsolution may be counteracting the thermal contraction. As the magma cools, volatiles exsolve and form bubbles, expanding the chamber. This would mean that a faster cooling magma chamber would contract less than expected. It is clear, however, that the surface deformation is very sensitive to changes in the temperature of the magma chamber.

5. Conclusions

Favàra Grande is an area of active degassing, and this CO_2 is focused along the faults that run through the area. The $\delta^{13}C$ of the CO_2, –7 ‰, is close to the magmatic $\delta^{13}C$ of –4 ‰, suggesting the source of the gas is mainly magmatic. Other surveys have shown a similar spacial pattern for methane, and other mineralisation was found around areas of high flux, reinforcing the view that a magma chamber is degassing along these faults. This of due to the lower permeability of the faults relative to unfractured. It is estimated that the permeability of the faults is 10^{-8}–10^{-9} cm^2.

The total CO_2 flux from the 0.163 km^2 surveyed is 1 300 kg d^{-1}, or 475 T yr^{-1}, at an average rate of 15.6 g m^{-2} d^{-1}. The flux rate changed over a period of a week, but meteorological effects make it difficult to draw conclusions about changes in the magmatic degassing rate. Past surveys have measured fluxes of 13 000 T yr^{-1} in 1998 and 2 100 T yr^{-1} in 2005, suggesting the flux is decreasing with time. However, with such a small data set it is impossible to tell if this trend is real or random variation, especially as the 1998 survey is likely to be an overestimate.

Although at least three inflationary events have occurred in the past thousand years, the island is currently deflating. This has been modelled as a point source contracting beneath Montagna Grande by 0.84×10^6 m^3. Such a point source is likely to be a magma chamber, as petrological data also places a magma chamber at about this depth. It is hard to explain the deflation using degassing alone. The measured CO_2 flux from Favàra escaping from a magma chamber would only cause a contraction of 690 m^3. Even if we assume most of the CO_2 escaping the chamber is not measured at the surface, we still require initial CO_2 concentrations in the magma to be over 1 wt%, or magma supply rates to be 25 times greater than the long-term rate estimated from eruption and chemical differentiation rates. Thermal contraction likely also plays a role, and the fact that the chamber is large and shallow means that small temperature changes lead to surface deformation. A cooling of

0.001 K $yr^{-}1$ would be enough to cause the measured deformation, ignoring the affects of volatiles.

Bibliography

Acocella, V., Cifelli, F., and Funiciello, R. (2001). The control of overburden thickness on resurgent domes: insights from analogue models. *Journal of Volcanology and Geothermal Research*, 111(1-4):137–153.

Badalamenti, B., Bruno, N., Caltabiano, T., Gangi, F. D., Giammanco, S., and Salerno, G. (2004). Continuous soil CO_2 and discrete plume SO_2 measurements at Mt. Etna (Italy) during 1997–2000: a contribution to volcano monitoring. *Bulletin of Volcanology*, 66(1):80–89.

Bagdassarov, N. S., Dingwell, D. B., and Wilding, M. C. (1996). Rhyolite magma degassing: an experimental study of melt vesiculation. *Bulletin of Volcanology*, 57(8):587–601.

Behncke, B., Berrino, G., Corrado, G., and Velardita, R. (2006). Ground deformation and gravity changes on the island of Pantelleria in the geodynamic framework of the Sicily Channel. *Journal of Volcanology and Geothermal Research*, 150(1-3):146–162.

Berrino, G. (1997). Gravity changes and present-day dynamics of the island of Pantelleria (Sicily Channel, Italy). *Journal of Volcanology and Geothermal Research*, 78(3-4):289–296.

Bonaccorso, A. and Mattia, M. (2000). Deflation acting on Pantelleria island (Sicily Channel) inferred through geodetic data. *Earth and Planetary Science Letters*, 180(1-2):91–101.

Bredehoeft, J. D. and Norton, D. L. (1990). Mass and energy transport in a deforming Earth's crust. In *The Role of Fluids in Crustal Processes*,

Studies in Geophysics, pages 27–41. National Academy Press, Washington, D.C.

Butler, G. W. (1892). Abstract of Mr. A. Ricco's account of the submarine eruption north-west of Pantelleria, October 1891. *Nature*, 45(1173):584–585.

Catalano, S., Guidi, G. D., Lanzafame, G., Monaco, C., and Tortorici, L. (2009). Late quaternary deformation on the island of Pantelleria: New constraints for the recent tectonic evolution of the Sicily Channel Rift (southern Italy). *Journal of Geodynamics*, 48(2):75–82.

Chiodini, G., Cioni, R., Guidi, M., Raco, B., and Marini, L. (1998). Soil CO_2 flux measurements in volcanic and geothermal areas. *Applied Geochemistry*, 13(5):543–552.

Civetta, L., Cornette, Y., Gillot, P. Y., and Orsi, G. (1988). The eruptive history of Pantelleria (Sicily Channel) in the last 50 ka. *Bulletin of Volcanology*, 50(1):47–57.

Civile, D., Lodolo, E., Tortorici, L., Lanzafame, G., and Brancolini, G. (2008). Relationships between magmatism and tectonics in a continental rift: The Pantelleria island region (Sicily Channel, Italy). *Marine Geology*, 251(1-2):32–46.

Cole, J., Milner, D., and Spinks, K. (2005). Calderas and caldera structures: a review. *Earth-Science Reviews*, 69(1-2):1–26.

Cooper, K. M., Reid, M. R., Murrell, M. T., and Clague, D. A. (2001). Crystal and magma residence at Kilauea volcano, Hawaii: ^{230}Th-^{226}Ra dating of the 1955 east rift eruption. *Earth and Planetary Science Letters*, 184(3-4):703–718.

Cornette, Y., Crisci, G., Gillot, P., and Orsi, G. (1983). Recent volcanic history of Pantelleria: A new interpretation. *Journal of Volcanology and Geothermal Research*, 17(1-4):361–373.

Craig, H. (1957). Isotopic standards for carbon and oxygen and correction factors for mass-spectrometric analysis of carbon dioxide. *Geochimica et Cosmochimica Acta*, 12(1-2):133–149.

D'Alessandro, W. (2007). Final report of research unit V3_7/02. Technical report, Istituto Nazionale di Geofisica e Vulcanologia, Sezione Palermo, Palermo, Italy.

D'Alessandro, W., Bellomo, S., Brusca, L., Fiebig, J., Longo, M., Martelli, M., Pecoraino, G., and Salerno, F. (2009). Hydrothermal methane fluxes from the soil at Pantelleria island (Italy). *Journal of Volcanology and Geothermal Research*, 187(3-4):147–157.

de Guidi, G. and Monaco, C. (2009). Late Holocene vertical deformation along the coast of Pantelleria island (Sicily Channel, Italy). *Quaternary International*, 206(1-2):158–165.

Favara, R., Giammanco, S., Inguaggiato, S., and Pecoraino, G. (2001). Preliminary estimate of CO_2 output from Pantelleria island volcano (Sicily, Italy): Evidence of active mantle degassing. *Applied Geochemistry*, 16(7-8):883–894.

Foerstner, H. (1881). Nota preliminare sulla geologia dell'isola di Pantelleria secondo gli studi fatti negli anni 1874 e 1881. *Bollettino del Reale Comitato Geologico Italiano*, 12:523–556.

Gianelli, G. and Grassi, S. (2001). Water-rock interaction in the active geothermal system of Pantelleria, Italy. *Chemical Geology*, 181(1-4):113–130.

Gioncada, A. and Landi, P. (2010). The pre-eruptive volatile contents of recent basaltic and pantelleritic magmas at Pantelleria (Italy). *Journal of Volcanology and Geothermal Research*, 189(1-2):191–201.

Granieri, D., Avino, R., and Chiodini, G. (2010). Carbon dioxide diffuse emission from the soil: ten years of observations at Vesuvio and Campi Flegrei

(Pozzuoli), and linkages with volcanic activity. *Bulletin of Volcanology*, 72(1):103–118.

Haining, R. (2003). *Spatial data analysis: Theory and practice*. Cambridge University Press, Cambridge.

Healy, R., Striegle, R., Russell, T., Hutchinson, G., and Livingston, G. (1996). Numerical evaluation of static-chamber measurements of soil-atmosphere gas exchange: Identification of physical processes. *Soil Science Society of America Journal*, 60:740–747.

Hollenstein, C., Kahle, H., Geiger, A., Jenny, S., Goes, S., and Giardini, D. (2003). New GPS constraints on the Africa-Eurasia plate boundary zone in southern Italy. *Geophysical Research Letters*, 30(18):1935.

Houghton, B., Weaver, S., Wilson, C., and Lanphere, M. (1992). Evolution of a quaternary peralkaline volcano: Mayor Island, New Zealand. *Journal of Volcanology and Geothermal Research*, 51(3):217–236.

Kuritani, T., Yokoyama, T., and Nakamura, E. (2007). Rates of thermal and chemical evolution of magmas in a cooling magma chamber: a chronological and theoretical study on basaltic and andesitic lavas from Rishiri volcano, Japan. *Journal of Petrology*, 48(7):1295–1319.

Lewicki, J. L., Hilley, G. E., Tosha, T., Aoyagi, R., Yamamoto, K., and Benson, S. M. (2007). Dynamic coupling of volcanic CO_2 flow and wind at the Horseshoe Lake tree kill, Mammoth Mountain, California. *Geophysical Research Letters*, 34:L03401.

LI-COR Inc (2007). *LI-8100 Automated Soil CO_2 Flux System & LI-8150 Multiplexer Instruction Manual*, 4 edition.

Lima, A., Vivo, B. D., Spera, F. J., Bodnar, R. J., Milia, A., Nunziata, C., Belkin, H. E., and Cannatelli, C. (2009). Thermodynamic model for uplift and deflation episodes (bradyseism) associated with magmatic-hydrothermal activity at the Campi Flegrei (Italy). *Earth-Science Reviews*, 97(1-4):44–58.

Lowenstern, J. (1994). Chlorine, fluid immiscibility, and degassing in peralkaline magmas from Pantelleria, Italy. *American Mineralogist*, 79(3-4):353–369.

MacDonald, R. (1974). Nomenclature and petrochemistry of the peralkaline oversaturated extrusive rocks. *Bulletin of Volcanology*, 38(2):498–516.

Macdonald, R. and Scaillet, B. (2006). The central Kenya peralkaline province: Insights into the evolution of peralkaline salic magmas. *Lithos*, 91(1-4):59–73.

Mahood, G. and Hildreth, W. (1983). Nested calderas and trapdoor uplift at Pantelleria, Strait of Sicily. *Geology*, 11(12):722–726.

Mahood, G. and Hildreth, W. (1986). Geology of the peralkaline volcano at Pantelleria, Strait of Sicily. *Bulletin of Volcanology*, 48(2-3):143–172.

Margari, V., Pyle, D., Bryant, C., and Gibbard, P. (2007). Mediterranean tephra stratigraphy revisited: Results from a long terrestrial sequence on Lesvos island, Greece. *Journal of Volcanology and Geothermal Research*, 163(1-4):34–54.

Mattia, M., Bonaccorso, A., and Guglielmino, F. (2007). Ground deformations in the island of Pantelleria (Italy): insights into the dynamic of the current intereruptive period. *Journal of Geophysical Research*, 112:B11406.

Molin, P., Acocella, V., and Funiciello, R. (2003). Structural, seismic and hydrothermal features at the border of an active intermittent resurgent block: Ischia island (Italy). *Journal of Volcanology and Geothermal Research*, 121(1-2):65–81.

Naumov, V., Solovova, I., Kovalenko, V., and Guzhova, A. (1989). Crystallization conditions and phase composition of melt inclusions in anorthoclase from Pantelleria agpaitic trachytes, Italy. *Geochemistry International*, 26(9):37–45.

Newman, S. and Lowenstern, J. (2002). VOLATILECALC: a silicate melt-H_2O-CO_2 solution model written in Visual Basic for Excel. *Computers and Geosciences*, 28(5):597–604.

Obrizzo, F., Gaudio, C. D., Ricco, C., Sepe, V., and Luongo, G. (1993). Pantelleria: ground deformation: Vertical ground movements. *Acta Vulcanologica*, 3:335.

Orsi, G., Gallo, G., and Zanchi, A. (1991). Simple-shearing block resurgence in caldera depressions. a model from Pantelleria and Ischia. *Journal of Volcanology and Geothermal Research*, 47(1-2):1–11.

Parello, F., Allard, P., D'Alessandro, W., Federico, C., Jean-Baptiste, P., and Catani, O. (2000). Isotope geochemistry of Pantelleria volcanic fluids, Sicily Channel rift: A mantle volatile end-member for volcanism in southern Europe. *Earth and Planetary Science Letters*, 180(3-4):325–339.

Reuther, C. and Eisbacher, G. (1985). Pantelleria Rift - crustal extension in a convergent intraplate setting. *Geologische Rundschau*, 74(3):585–597.

Scheibner, B., Heumann, A., Wörner, G., and Civetta, L. (2008). Crustal residence times of explosive phonolite magmas: U-Th ages of magmatic Ca-garnets of Mt. Somma-Vesuvius (Italy). *Earth and Planetary Science Letters*, 276(3-4):293–301.

Squarci, P., Gianelli, G., Grassi, S., Mussi, M., and D'Amore, F. (1994). Preliminary results of geothermal prospecting on the island of Pantelleria (Italy). *Acta Vulcanologica*, 5:117–123.

SRTM (2007). Shuttle Radar Topography Mission. http://www2.jpl.nasa.gov/srtm/.

Tomiya, A. and Takahashi, E. (1995). Reconstruction of an evolving magma chamber beneath Usu volcano since the 1663 eruption. *Journal of Petrology*, 36(3):617–636.

Turner, S., Foden, J., George, R., Evans, P., Varne, R., Elburg, M., and Jenner, G. (2003). Rates and processes of potassic magma evolution beneath Sangeang Api volcano, east Sunda Arc, Indonesia. *Journal of Petrology*, 44(3):491–515.

Villari, L. (1970). The caldera of Pantelleria. *Bulletin of Volcanology*, 34(3):758–766.

Villari, L. (1974). The island of Pantelleria. *Bulletin of Volcanology*, 38(2):680–724.

White, J. C., Parker, D. F., and Ren, M. (2009). The origin of trachyte and pantellerite from Pantelleria, Italy: Insights from major element, trace element, and thermodynamic modelling. *Journal of Volcanology and Geothermal Research*, 179(1-2):33–55.

Wright, J. (1980). Stratigraphy and geology of the welded air-fall tuffs of Pantelleria, Italy. *Geologische Rundschau*, 69(1):263–291.

Appendix A:
CO_2 Flux Survey Measurements

Table A.1: List of all CO_2 flux measurements. For locations see figure A.1

No	UTM Grid	Coordinates		Date	Time	CO_2 Flux /g m^{-2} d^{-1}	Temperature/°C Initial	Range
15	QF	67656	73408	–	–	1902.69	–	–
23	QF	67383	73648	31/08/2009	11:10	17.45	30.15	1.46
26	TA	32365	73446	31/08/2009	12:06	0.00	30.25	1.82
27	TA	32426	73575	02/09/2009	07:24	0.00	22.97	0.22
28	TA	32443	73545	02/09/2009	07:35	10.87	23.12	0.09
29	TA	32403	73547	02/09/2009	07:48	0.00	23.47	0.37
30	TA	32415	73521	02/09/2009	07:59	7.49	23.74	0.19
31	TA	32415	73492	02/09/2009	08:10	0.00	23.96	0.09
32	TA	32427	73476	02/09/2009	08:21	0.00	24.11	0.41
33	TA	32442	73462	02/09/2009	08:41	0.00	24.45	0.59
34	TA	32442	73462	02/09/2009	08:50	0.00	24.67	0.24
35	TA	32427	73445	02/09/2009	09:05	13.31	25.34	0.73
36	TA	32412	73460	02/09/2009	09:27	0.00	27.33	1.16
37	TA	32403	73482	02/09/2009	09:27	44.18	27.51	0.28
38	TA	32395	73498	02/09/2009	09:38	21.41	27.35	1.56
39	TA	32379	73464	02/09/2009	09:49	35.17	29.03	1.98
40	TA	32379	73464	02/09/2009	10:00	9.89	31.51	2.04
41	TA	32384	73424	02/09/2009	10:11	24.45	30.73	0.93
42	TA	32384	73424	02/09/2009	10:20	31.33	30.65	1.37
43	TA	32372	73410	02/09/2009	10:32	0.00	31.35	1.64
44	TA	32349	73404	02/09/2009	10:43	27.11	30.83	2.32
45	TA	32341	73395	02/09/2009	10:55	0.00	32.65	1.60
46	TA	32356	73391	02/09/2009	11:06	17.76	32.30	1.42
47	TA	32356	73391	02/09/2009	11:14	20.30	32.10	0.97
48	TA	32393	73378	02/09/2009	11:27	0.00	31.79	1.07
49	TA	32341	73379	02/09/2009	11:39	87.57	30.68	2.08
50	TA	32356	73364	02/09/2009	11:50	0.00	32.56	0.69
51	TA	32342	73372	02/09/2009	11:59	0.00	31.77	1.40
52	TA	32336	73357	02/09/2009	12:10	0.00	30.86	1.33
53	TA	32347	73355	02/09/2009	12:23	0.00	31.25	1.11
54	TA	32326	73355	02/09/2009	12:34	0.00	32.91	0.56
55	TA	32323	73343	02/09/2009	12:44	0.00	31.98	1.73
56	TA	32369	73297	02/09/2009	12:56	45.21	32.32	0.72
57	TA	32369	73297	02/09/2009	13:04	44.60	32.42	0.61
58	TA	32371	73310	02/09/2009	13:53	70.92	32.70	1.59
59	TA	32379	73298	02/09/2009	14:04	0.00	30.94	2.13

Table A.1: Continued...

No	UTM Grid	Coordinates		Date	Time	CO_2 Flux /g m^{-2} d^{-1}	Temperature/°C Initial	Range
60	TA	32374	73286	02/09/2009	14:14	0.00	31.94	1.38
61	TA	32356	73303	02/09/2009	14:23	0.04	32.21	1.63
62	TA	32374	73317	02/09/2009	14:33	0.00	32.80	2.93
63	TA	32378	73311	02/09/2009	14:44	24.49	31.26	1.59
64	TA	32355	73285	02/09/2009	14:55	0.04	33.11	1.27
65	TA	32401	73563	03/09/2009	07:23	36.77	22.48	0.37
66	TA	32381	73573	03/09/2009	07:33	23.38	22.74	0.05
67	TA	32381	73573	03/09/2009	07:41	24.53	22.79	0.06
68	TA	32368	73575	03/09/2009	07:51	0.00	22.99	0.16
69	TA	32349	73581	03/09/2009	08:00	0.00	23.24	0.11
70	TA	32326	73606	03/09/2009	08:08	0.00	23.74	0.74
71	TA	32310	73592	03/09/2009	08:16	0.00	24.86	1.02
72	TA	32327	73577	03/09/2009	08:23	0.00	26.26	0.63
73	TA	32353	73564	03/09/2009	08:34	0.00	26.74	0.14
74	TA	32373	73555	03/09/2009	09:02	40.95	25.87	0.06
75	TA	32390	73547	03/09/2009	09:11	83.08	27.53	1.64
76	TA	32390	73547	03/09/2009	09:18	83.77	29.44	1.31
77	TA	32376	73529	03/09/2009	09:27	44.11	29.45	1.53
78	TA	32376	73529	03/09/2009	09:35	43.31	29.83	0.90
79	TA	32353	73552	03/09/2009	09:44	48.29	29.43	1.20
80	TA	32315	73576	03/09/2009	09:52	0.00	30.52	1.26
81	TA	32298	73552	03/09/2009	10:01	0.00	31.30	1.19
82	TA	32280	73520	03/09/2009	10:10	0.00	31.30	1.30
83	TA	32307	73489	03/09/2009	10:18	0.00	32.09	0.98
84	TA	32330	73508	03/09/2009	10:26	12.81	31.24	0.95
85	TA	32330	73508	03/09/2009	10:33	9.96	31.67	1.05
86	TA	32343	73519	03/09/2009	10:41	131.91	32.06	1.14
87	TA	32359	73506	03/09/2009	10:50	40.61	32.00	1.45
88	TA	32373	73494	03/09/2009	10:58	11.26	33.36	1.07
89	TA	32360	73476	03/09/2009	11:07	27.76	34.94	1.21
90	TA	32357	73482	03/09/2009	11:15	22.70	35.12	1.04
91	TA	32335	73494	03/09/2009	11:23	46.66	34.91	0.94
92	TA	32334	73482	03/09/2009	11:31	5.97	34.53	1.14
93	TA	32344	73471	03/09/2009	11:39	24.45	33.56	1.07
94	TA	32344	73471	03/09/2009	11:46	26.08	33.94	0.80
95	TA	32340	73451	03/09/2009	11:54	136.39	33.09	0.95
96	TA	32322	73461	03/09/2009	12:02	15.44	30.60	0.80
97	TA	32304	73485	03/09/2009	12:10	0.00	31.96	1.44
98	TA	32307	73461	04/09/2009	07:57	34.07	25.19	0.58
99	TA	32305	73437	04/09/2009	08:09	2.59	25.50	0.22
100	TA	32285	73434	04/09/2009	08:17	7.68	25.91	0.45
101	TA	32285	73434	04/09/2009	08:24	8.40	26.39	0.36
102	TA	32273	73450	04/09/2009	08:33	0.00	27.36	0.96
103	TA	32248	73476	04/09/2009	08:41	16.77	27.88	0.93

Table A.1: Continued...

No	UTM Grid	Coordinates		Date	Time	CO_2 Flux /g m^{-2} d^{-1}	Temperature/°C Initial	Range
104	TA	32229	73466	04/09/2009	08:50	13.12	28.01	0.66
105	QF	67772	73493	04/09/2009	08:58	0.00	28.41	0.64
106	TA	32239	73443	04/09/2009	09:06	2.09	29.12	0.96
107	QF	67783	73437	04/09/2009	09:14	0.00	29.91	0.78
108	QF	67771	73495	04/09/2009	09:23	2.55	30.05	1.20
109	QF	67755	73489	04/09/2009	09:31	0.00	30.78	0.75
110	QF	67729	73480	04/09/2009	09:39	0.00	30.59	1.46
111	QF	67747	73455	04/09/2009	09:47	0.00	31.24	0.69
112	QF	67744	73428	04/09/2009	09:54	0.00	32.26	1.16
113	QF	67727	73428	04/09/2009	10:02	1.90	33.36	0.81
114	QF	67727	73428	04/09/2009	10:09	1.75	33.66	0.78
115	QF	67703	73445	04/09/2009	10:19	0.27	32.74	0.92
116	QF	67740	73415	04/09/2009	10:28	1.22	33.30	1.29
117	QF	67765	73421	04/09/2009	10:36	1.06	33.83	1.32
118	TA	32221	73425	04/09/2009	10:44	13.08	35.27	2.47
119	TA	32236	73427	04/09/2009	10:52	5.82	35.93	1.11
120	TA	32252	73428	04/09/2009	11:00	11.71	35.57	1.93
121	TA	32269	73426	04/09/2009	11:08	5.82	35.93	1.14
122	TA	32290	73426	04/09/2009	11:17	22.32	35.30	1.60
123	TA	32290	73426	04/09/2009	11:23	22.59	36.57	0.83
124	TA	32310	73428	04/09/2009	11:33	14.56	35.67	1.11
125	TA	32330	73430	04/09/2009	11:42	19.32	35.25	1.05
126	TA	32326	73409	04/09/2009	11:49	14.53	34.95	2.24
127	TA	32305	73408	04/09/2009	11:57	26.05	36.12	1.82
128	TA	32305	73408	04/09/2009	12:04	25.86	36.52	0.84
129	TA	32281	73406	04/09/2009	12:12	13.65	36.02	1.09
130	TA	32251	73397	04/09/2009	17:06	14.18	31.48	1.07
131	TA	32220	73401	04/09/2009	17:15	3.84	32.57	1.16
132	QF	67750	73384	04/09/2009	17:23	0.00	31.99	0.48
133	QF	67750	73384	04/09/2009	–	1.67	–	–
134	QF	67759	73356	04/09/2009	17:35	5.63	30.42	0.26
135	QF	67726	73346	04/09/2009	17:44	0.23	29.06	0.23
136	QF	67775	73351	04/09/2009	17:53	56.31	28.79	0.51
137	QF	67775	73351	04/09/2009	17:59	57.72	29.24	0.25
138	TA	32239	73363	04/09/2009	18:07	13.69	29.56	1.00
139	TA	32248	73354	04/09/2009	18:15	144.76	30.10	1.08
140	TA	32268	73361	04/09/2009	18:23	212.97	29.45	0.78
141	TA	32268	73361	04/09/2009	18:29	224.30	29.91	0.31
142	TA	32307	73348	04/09/2009	18:28	1.94	28.68	0.39
143	TA	32298	73325	04/09/2009	18:45	51.87	28.39	0.17
144	TA	32265	73326	04/09/2009	18:53	97.87	28.23	0.43
145	TA	32225	73329	04/09/2009	19:01	24.49	28.32	0.66
146	TA	32216	73333	04/09/2009	19:09	9.85	27.87	0.18
147	QF	67231	73727	05/09/2009	07:26	8.67	22.40	0.13

Table A.1: Continued...

No	UTM Grid	Coordinates		Date	Time	CO_2 Flux /g m^{-2} d^{-1}	Temperature/°C Initial	Range
148	QF	67231	73727	05/09/2009	07:54	5.21	22.69	0.29
149	QF	67245	73714	05/09/2009	08:03	15.02	23.94	0.80
150	QF	67270	73706	05/09/2009	08:11	20.95	24.53	0.45
151	QF	67255	73697	05/09/2009	08:19	138.86	25.10	1.11
152	QF	67255	73697	05/09/2009	08:26	134.26	25.54	1.32
153	QF	67264	73680	05/09/2009	08:37	37.53	26.09	1.32
154	QF	67279	73697	05/09/2009	08:49	4.83	25.75	0.85
155	QF	67279	73673	05/09/2009	08:57	2.59	27.03	2.24
156	QF	67294	73693	05/09/2009	09:06	7.91	28.72	0.31
157	QF	67304	73701	05/09/2009	09:14	7.03	28.12	1.11
158	QF	67319	73725	05/09/2009	09:22	1.29	28.15	1.12
159	QF	67342	73718	05/09/2009	09:29	1.86	28.55	0.82
160	QF	67334	73693	05/09/2009	09:37	3.38	27.61	1.62
161	QF	67302	73667	05/09/2009	09:44	2.93	28.37	1.87
163	QF	67309	73634	05/09/2009	–	4.49	–	–
164	QF	67320	73646	05/09/2009	–	2.81	–	–
165	QF	67360	73659	05/09/2009	10:10	6.12	29.38	0.69
166	QF	67371	73677	05/09/2009	10:24	1.25	29.16	0.61
167	QF	67391	73702	05/09/2009	10:32	2.78	29.08	1.36
168	QF	67404	73670	05/09/2009	10:40	0.84	30.13	0.96
169	QF	67391	73662	05/09/2009	10:47	2.81	30.68	1.00
170	QF	67378	73640	05/09/2009	10:54	107.57	29.46	0.74
171	QF	67365	73615	05/09/2009	11:01	27.19	28.33	1.38
172	QF	67347	73592	05/09/2009	11:09	47.99	30.89	1.31
173	QF	67347	73592	05/09/2009	11:15	50.42	32.33	0.92
174	QF	67360	73577	05/09/2009	11:23	30.53	31.52	1.06
175	QF	67381	73600	05/09/2009	11:30	97.80	30.78	2.30
176	QF	67386	73621	05/09/2009	11:37	263.47	30.54	1.24
177	QF	67406	73637	05/09/2009	11:43	33.88	30.55	1.34
178	QF	67423	73656	05/09/2009	11:50	0.80	31.45	1.12
179	QF	67433	73638	05/09/2009	11:58	0.42	32.97	1.36
180	QF	67421	73619	05/09/2009	12:05	11.90	33.97	1.08
181	QF	67421	73619	05/09/2009	12:11	12.47	35.41	0.14
182	QF	67408	73583	05/09/2009	17:45	1.37	27.29	0.75
183	QF	67394	73568	05/09/2009	17:54	26.65	27.12	0.79
184	QF	67380	73561	05/09/2009	18:01	179.17	26.61	0.89
185	QF	67375	73547	05/09/2009	18:09	2.55	26.08	0.63
186	QF	67396	73531	05/09/2009	18:16	26.81	25.51	0.28
187	QF	67414	73543	05/09/2009	18:23	28.21	25.30	0.31
188	QF	67442	73564	05/09/2009	18:30	0.30	25.34	0.65
189	QF	67455	73541	05/09/2009	18:37	9.09	25.07	0.26
190	QF	67440	73529	05/09/2009	18:44	19.20	25.02	0.48
191	QF	67416	73507	05/09/2009	18:52	14.15	24.75	0.33
192	QF	67435	73495	05/09/2009	18:59	1.10	24.22	0.17

Table A.1: Continued...

No	UTM Grid	Coordinates		Date	Time	CO_2 Flux /g m^{-2} d^{-1}	Temperature/°C Initial	Range
193	QF	67455	73498	06/09/2009	07:59	16.69	22.54	0.38
194	QF	67479	73522	06/09/2009	08:07	12.47	22.31	0.28
195	QF	67507	73507	06/09/2009	08:14	6.16	22.22	0.29
196	QF	67507	73507	06/09/2009	08:21	4.41	22.40	0.16
197	QF	67488	73491	06/09/2009	08:29	0.38	23.17	0.51
198	QF	67465	73472	06/09/2009	08:37	0.27	23.14	0.08
199	QF	67488	73454	06/09/2009	08:45	0.87	23.67	0.35
200	QF	67529	73443	06/09/2009	08:53	0.19	23.99	0.31
201	QF	67559	73437	06/09/2009	09:00	0.38	23.91	0.58
202	QF	67529	73435	06/09/2009	09:07	0.42	24.20	0.74
203	QF	67595	73462	06/09/2009	09:14	0.68	24.69	0.55
204	QF	67531	73471	06/09/2009	09:21	3.27	25.35	1.00
205	QF	67548	73466	06/09/2009	09:28	0.99	26.06	0.99
206	QF	67524	73473	06/09/2009	09:35	0.38	26.27	0.92
207	QF	67622	73452	06/09/2009	09:45	3.73	25.71	0.90
208	QF	67622	73452	06/09/2009	09:51	3.50	26.26	0.68
209	QF	67636	73475	06/09/2009	09:58	20.99	26.02	1.25
210	QF	67615	73422	06/09/2009	10:08	6.62	26.80	0.99
211	QF	67613	73399	06/09/2009	10:19	10.84	26.83	1.27
212	QF	67596	73395	06/09/2009	10:26	0.91	28.72	1.10
213	QF	67601	73407	06/09/2009	10:36	1.10	28.79	0.36
214	QF	67632	73423	06/09/2009	10:50	163.12	29.84	2.54
215	QF	67632	73423	06/09/2009	10:56	165.37	33.20	1.00
216	QF	67632	73409	06/09/2009	11:05	63.50	33.38	1.48
216	QF	67632	73409	06/09/2009	11:11	64.83	35.43	0.74
218	QF	67635	73393	06/09/2009	11:21	60.99	32.95	1.19
219	QF	67648	73492	06/09/2009	11:39	15.17	31.83	2.24
220	QF	67659	73388	06/09/2009	11:48	9.62	31.04	1.49
221	QF	67671	73391	06/09/2009	11:56	12.89	31.03	1.57
222	QF	67674	73430	06/09/2009	12:06	38.14	30.85	0.95
223	QF	67683	73423	06/09/2009	12:14	18.75	31.46	0.48
252	QF	67305	73594	–	–	13.73	–	–
253	QF	67320	73576	–	–	20.50	–	–
254	QF	67332	73562	–	–	6.73	–	–
255	QF	67349	73544	–	–	76.35	–	–
256	QF	67371	73527	–	–	21.64	–	–
257	QF	67393	73510	–	–	16.46	–	–
258	QF	67424	73486	–	–	5.93	–	–
259	QF	67467	73463	–	–	0.65	–	–
260	QF	67462	73447	–	–	2.24	–	–
262	TA	32390	73582	10/09/2009	08:43	83.43	–	–
263	TA	32372	73534	10/09/2009	08:54	134.38	18.90	0.08
264	TA	32343	73581	10/09/2009	09:10	19.20	19.30	0.20
265	TA	32279	73386	10/09/2009	09:28	35.86	19.65	0.21

Table A.1: Continued...

No	UTM Grid	Coordinates		Date	Time	CO_2 Flux /g m^{-2} d^{-1}	Temperature/°C Initial	Range
266	TA	32275	73449	10/09/2009	09:42	37.76	22.47	0.65
267	TA	32221	73423	10/09/2009	09:53	47.42	24.02	0.26
268	QF	67633	73410	10/09/2009	10:19	35.36	22.10	0.11
269	QF	67631	73410	10/09/2009	10:26	103.96	22.40	0.16
270	QF	67551	73501	10/09/2009	10:37	27.26	23.58	0.15
271	QF	67455	73503	10/09/2009	10:50	272.37	24.33	0.22
272	QF	67455	73503	10/09/2009	10:58	230.05	24.87	0.47
273	QF	67387	73558	10/09/2009	11:07	255.79	24.65	0.76
274	QF	67386	73598	10/09/2009	11:16	187.16	24.63	0.41
275	QF	67349	73623	10/09/2009	11:27	69.28	24.65	0.47
276	QF	67316	73666	10/09/2009	11:35	25.82	25.00	0.36
277	QF	67266	73681	10/09/2009	11:44	68.52	24.92	0.75

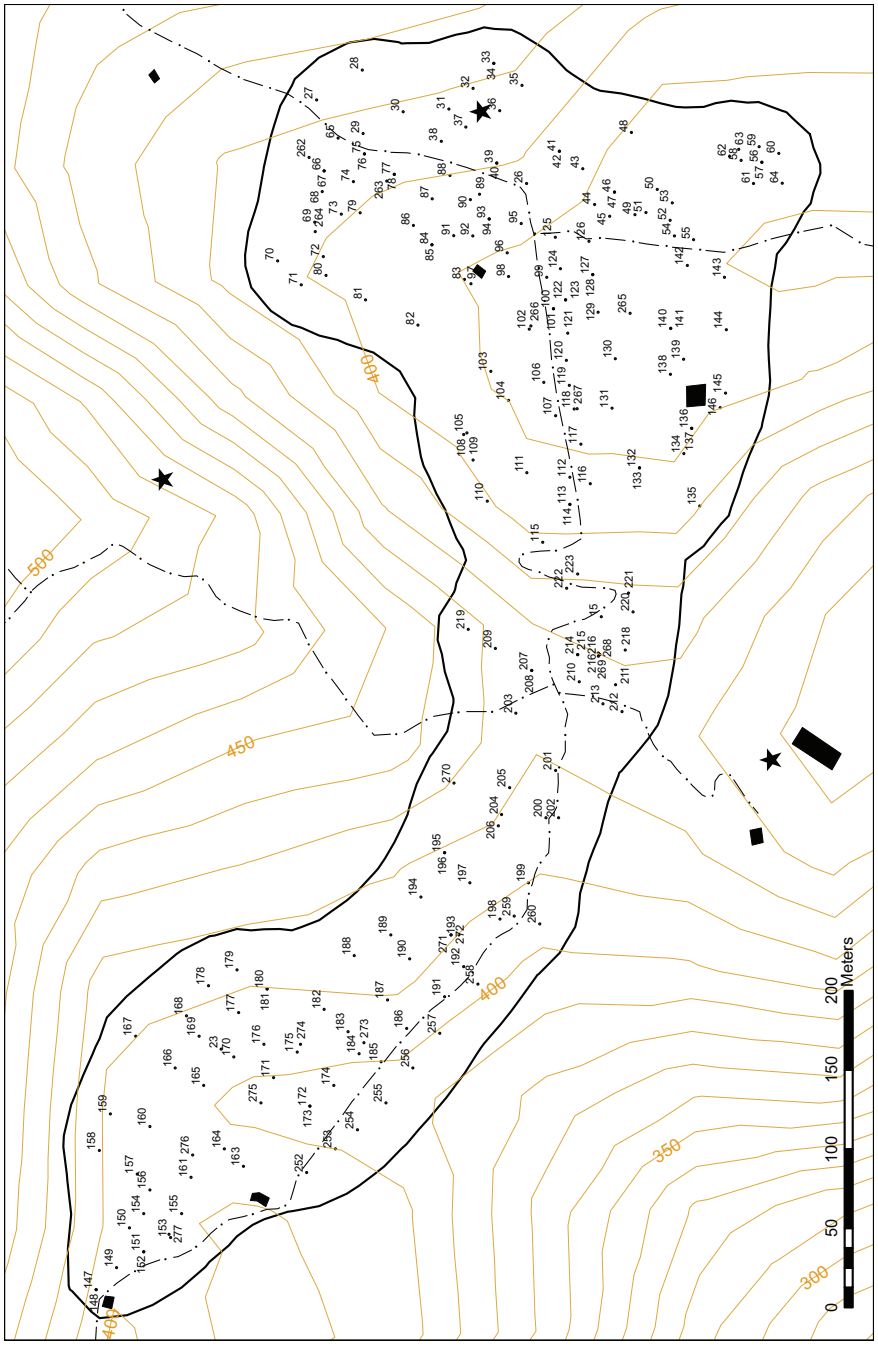

Figure A.1: Map showing the location of survey sites.

Appendix B:
Poster

[Fold Out]

Appendix C:
Original Project Proposal

Pantelleria Island Volcano I: links between volcanism and tectonics

Supervisor: Marie Edmonds

Pantelleria Island is the exposed portion of a partly submerged, dormant volcano in the Sicily Channel, 70 km north of Tunisia. It is located on African continental crust, within a NW-SE-trending rift system developed during the Neogene–Quaternary in the Pelagian Block. The rift is still active and the NW-SE trending strike-slip faults that form it are connected with N-S normal faults producing pull-apart basins (Civile et al., 2008). These structures have influenced strongly the location of volcanic activity on the island. The geologic evolution of Pantelleria has been described in detail and most of the erupted products have been dated (Mahood and Hildreth, 1986). Significant hazards exist and may affect people in the region, from both earthquakes and volcanic eruptions; the last eruption was in 1891, offshore. The only evidence of ongoing magmatic evolution and degassing beneath the island is in the form of CO_2 emissions (Favara et al., 2001).

This project will investigate the links between volcanic centres and tectonic structures on the island during a period of fieldwork on Pantelleria, for which the student must find funds. The specific objectives will be a) to constrain the location and nature of the faults on the island and b) map the emission of CO_2 gas to evaluate the relationship between outgassing and structural features. This project would suit a student interested in volcanology, geochemistry and tectonics. The project requires precise and detailed observations in the field, as well as the use of field-portable gas measurement

equipment, for which training will be provided.

Mahood, G. E. and W. Hildreth, 1986. Geology of the peralkaline volcano at Pantelleria, Strait of Sicily. Bulletin of Volcanology 48:143-172.

Civile, D., Lodolo, E., Tortorici, L., Lanzafame, G., Brancolini, G., 2008. Relationships between magmatism and tectonics in a continental rift: The Pantelleria Island region (Sicily Channel, Italy). Marine Geology 251, 1-2, 32-46.

Favara, R., Giammanco, S., Inguaggiato, S., Pecoraino, G., 2001. Preliminary estimate of CO_2 output from Pantelleria Island volcano (Sicily, Italy): evidence of active mantle degassing. Appl. Geochem. 16, 883-894.

Appendix D: Self-Assessment

The project went well. Collecting the data over the summer allowed plenty of time for analysis during the term. I went with another student, David Neave, who was collecting rock samples for his project. This was useful as he could drive and I couldn't.

My supervisor, Marie Edmonds, came with us for the first few days to show us round the island and to train me with the LI-8100 Automated Soil CO_2 Flux System used in the field. Richard Herd also came along, and as he had worked on Pantelleria before he was a useful guide. Back in Cambridge, Marie held regular meetings with me during term-time, and was generally very helpful.

While there was a fair amount of literature on the island, because of the unusual chemistry of the pantellerites it was sometimes hard to find the necessary data. There is little information on the solubility of volatiles such as water and CO_2 in highly peralkaline rocks. There was also no information on the initial concentration of CO_2 which was an important part of my analysis.

The largest problem with this project was in trying to relate the deformation to probable causes. There are no previous models relating cooling and degassing directly to the deformation. Such a model was too complex to be created during the time I had, so I had to rely on more basic calculations. There is great scope for improving on this, and there are several PhDs advertised this year that aim to do this.

Overall I feel this project has met its goals, and would recommend similar projects in the future. Funding was an issue, most of it was funded out of my own pocket. Despite this, I greatly enjoyed being able to work on an active volcano, and I hope to continue to do something similar after I finish in Cambridge at the end of the year.